

RESEARCH

Open Access



# *Drosophila* CASK regulates brain size and neuronal morphogenesis, providing a genetic model of postnatal microcephaly suitable for drug discovery

Judith A. Tello<sup>1,2,3</sup> , Linan Jiang<sup>4</sup> , Yitshak Zohar<sup>4,5,6</sup> and Linda L. Restifo<sup>1,2,6,7\*</sup>

## Abstract

**Background** *CASK*-related neurodevelopmental disorders are untreatable. Affected children show variable severity, with microcephaly, intellectual disability (ID), and short stature as common features. X-linked human *CASK* shows dosage sensitivity with haploinsufficiency in females. *CASK* protein has multiple domains, binding partners, and proposed functions at synapses and in the nucleus. Human and *Drosophila* *CASK* show high amino-acid-sequence similarity in all functional domains. Flies homozygous for a hypomorphic *CASK* mutation ( $\Delta 18$ ) have motor and cognitive deficits. A *Drosophila* genetic model of *CASK*-related disorders could have great scientific and translational value.

**Methods** We assessed the effects of *CASK* loss of function on morphological phenotypes in *Drosophila* using established genetic, histological, and primary neuronal culture approaches. NeuronMetrics software was used to quantify neurite-arbor morphology. Standard nonparametric statistics methods were supplemented by linear mixed effects modeling in some cases. Microfluidic devices of varied dimensions were fabricated and numerous fluid-flow parameters were used to induce oscillatory stress fields on CNS tissue. Dissociation into viable neurons and neurite outgrowth in vitro were assessed.

**Results** We demonstrated that  $\Delta 18$  homozygous flies have small brains, small heads, and short bodies. When neurons from developing *CASK*-mutant CNS were cultured in vitro, they grew small neurite arbors with a distinctive, quantifiable “bushy” morphology that was significantly rescued by transgenic *CASK*<sup>+</sup>. As in humans, the bushy phenotype showed dosage-sensitive severity. To overcome the limitations of manual tissue trituration for neuronal culture, we optimized the design and operation of a microfluidic system for standardized, automated dissociation of CNS tissue into individual viable neurons. Neurons from *CASK*-mutant CNS dissociated in the microfluidic system recapitulate the bushy morphology. Moreover, for any given genotype, device-dissociated neurons grew larger arbors than did manually dissociated neurons. This automated dissociation method is also effective for rodent CNS.

**Conclusions** These biological and engineering advances set the stage for drug discovery using the *Drosophila* model of *CASK*-related disorders. The bushy phenotype provides a cell-based assay for compound screening. Nearly a dozen genes encoding *CASK*-binding proteins or transcriptional targets also have brain-development mutant phenotypes, including ID. Hence, drugs that improve *CASK* phenotypes might also benefit children with disorders due to mutant *CASK* partners.

\*Correspondence:

Linda L. Restifo

LLR@arizona.edu

Full list of author information is available at the end of the article



© The Author(s) 2023. **Open Access** This article is licensed under a Creative Commons Attribution 4.0 International License, which permits use, sharing, adaptation, distribution and reproduction in any medium or format, as long as you give appropriate credit to the original author(s) and the source, provide a link to the Creative Commons licence, and indicate if changes were made. The images or other third party material in this article are included in the article's Creative Commons licence, unless indicated otherwise in a credit line to the material. If material is not included in the article's Creative Commons licence and your intended use is not permitted by statutory regulation or exceeds the permitted use, you will need to obtain permission directly from the copyright holder. To view a copy of this licence, visit <http://creativecommons.org/licenses/by/4.0/>. The Creative Commons Public Domain Dedication waiver (<http://creativecommons.org/publicdomain/zero/1.0/>) applies to the data made available in this article, unless otherwise stated in a credit line to the data.

**Keywords** Intellectual disability, Haploinsufficiency, Short stature, Primary neuronal culture, Neurite arbor, Neurogenetics, Microfluidics, Immunostaining

## Background

Originally identified as a neurexin-binding protein [53], CASK has numerous partners, each of which binds to one of its seven functional domains or motifs [106] (Fig. 1a, Additional file: Table A1). As more binding partners were discovered, it was proposed that CASK acts as a nucleation site, or scaffold, to aggregate proteins at specific subcellular sites [16]. In neurons, CASK localizes to both pre- and postsynaptic zones, as well as to the nucleus where it contributes to transcriptional regulation [59], Additional file: Table A1). CASK is regulated via phosphorylation by at least two kinases, CDK5 and PKA, which impacts its subcellular localization and function [62, 135]. CASK later emerged as essential for human brain development [102, 112].

Over 230 unique patients with mutations in the X-linked *CASK* gene (MIM# 300172; <https://omim.org/entry/300172>, last accessed 9 February 2023) have been reported, with five continents and many ancestries represented (Additional file: Table A2). Pathogenic loss-of-function (LOF) *CASK* mutations are found in all protein-coding domains [57]. Some mutant proteins had reduced binding to neurexin or other partners [79–81, 119, 151, 157]. Many genes encoding *CASK* transcriptional targets or partners also have neurodevelopmental mutant phenotypes (Additional file: Table A1). In network terms, *CASK* is the hub of a set of genes essential for brain development.

*CASK*-related neurodevelopmental disorders span a wide range of phenotypic severity. At the low end of the range is isolated or syndromic intellectual disability (ID), mostly but not exclusively in males and often accompanied by nystagmus (MIM# 300422; <https://omim.org/entry/300422>, last accessed 9 February 2023) [29, 34, 52, 124, 150]. Some of these patients have postnatal

microcephaly. At the high end of the range is microcephaly with pontine-cerebellar hypoplasia (MICPCH, MIM# 300749; <https://omim.org/entry/300749>, last accessed 9 February 2023), a congenital disorder that causes severe psychomotor delay, often with early-onset, hard-to-control epilepsy, optic nerve/retinal abnormalities, and/or short stature. These patients have de novo germline *CASK* mutations, and most but not all are heterozygous females [47, 49, 55–57, 71, 80, 100, 103, 104, 112, 113, 120, 128, 129, 149, 153, 160]. In other cases, the phenotypes do not fit neatly into either category, including autism spectrum disorder (ASD) without ID in males or females [10, 64, 139], progressive microcephaly without cerebellar/pontine abnormalities [24], or focal cortical dysplasia in a female with a large somatic *CASK*-mutant clone [83]. With 41% of *CASK* clinical cases published in 2021 or later (Additional file: Table A2), many with novel mutations and phenotypes, it seems likely that the full phenotypic spectrum of *CASK*-related disorders remains to be revealed.

Several lines of evidence indicate that human brain development is very sensitive to *CASK* dosage and level of function. First, *CASK* shows haploinsufficiency, i.e., a single wild-type copy does not provide normal function in females. Females with ~50% of normal gene dosage due to heterozygous de novo germline whole-gene deletions, are most often born with MICPCH. Second, male infants with MICPCH are relatively rare, clinically very severe, dying as neonates or children [112, 120, 151]. Some surviving male patients with de novo mutations and MICPCH show somatic mosaicism [15, 57, 103], which would reduce the deleterious impact. The early lethality of the most severely affected males, along with the sex ratio of reported cases (F:M=2.19, Additional file: Table A2) suggests that a significant fraction

(See figure on next page.)

**Fig. 1** *Drosophila* *CASK* gene, proteins, and genetic reagents. **a** Color-coded schematic, drawn to scale, showing identical organization of *CASK* protein domains in *H. sapiens* and *D. melanogaster*. Amino-acid (aa) sequence similarity (%) as indicated; identities are CaMK-like 68%; L27A 31%; L27B 45%; PDZ 82%; SH3 67%; GUK 70%. The white boxes between SH3 and GUK are the "hook" motif. **b** Cytogenetic and molecular maps of *CASK* (FlyBase ID FBgn0013759; <https://flybase.org/reports/FBgn0013759>, last accessed 6 February 2023). Region 93F10-12 on right arm of chromosome 3 [86], reproduced in [91], centromere to the left. *CASK* gene span: genomic DNA map 21,783 – 21,822 kb (Fly Base, FB2022\_06); scale at top right applies to all maps in (b)-(d). Protein orientation in (a) is flipped 180° relative to transcription direction. *CASK* (blue), with two transcriptional start sites (left-pointing arrows), and *tsl* (green) genes. P-element *EY07081* insertion site in first intron. Two overlapping chromosomal deficiencies delete *CASK* DNA, with breakpoints estimated by restriction mapping [96]. **c** *CASK* alleles [142]. Imprecise excision of *EY07081* generated *CASK* mutation,  $\Delta 18$ , with deletion of exons 1 and 2, and insertion of small piece of *roo* transposon at the breakpoint. Precise excision yielded *Ex33*, which serves as the control allele. **d** Endogenous and engineered *CASK* transcripts. Boxes represent exons; color scheme for encoded protein domains as in (a), gray for 5'- and 3'-untranslated regions. *CASK*- $\beta$  is the full-length transcript; internal promoter generates short transcript, *CASK*- $\alpha$ , which is missing the 5' exons. The *UAS-CASK*<sup>+</sup> 10.20 construct expresses full-length wild-type *CASK* cDNA under UAS control

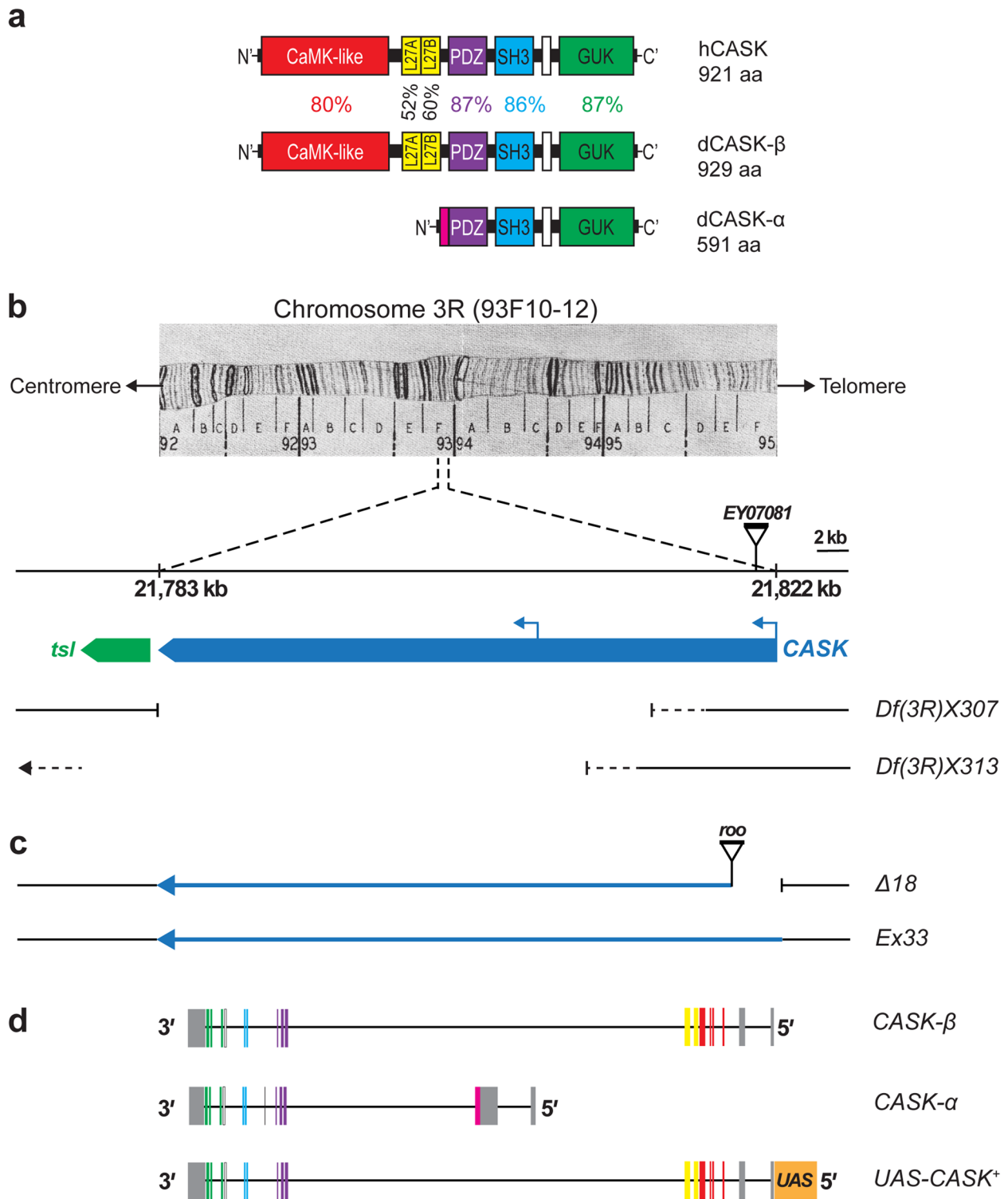


**Fig. 1** (See legend on previous page.)

of males with germline de novo *CASK*-null mutations die either in utero or very young without a molecular diagnosis [103, 112]. In other words, *CASK* is likely

an essential gene in humans, as it is in mice [8]. Third, weak *CASK*-LOF mutations, i.e., allowing considerable retention of function, cause X-linked recessive ID in

males [10, 34, 52, 111, 124, 139, 150] with normal brain architecture (at MRI resolution) and variable features, including nystagmus, disruptive behavior, autism, constipation, facial dysmorphic, short stature, and microcephaly or relative macrocephaly. Those mutations may be inherited from a heterozygous or somatic-mosaic mother who was either very mildly affected or phenotypically normal [139, 151]. Taken together, the data are most consistent with MICPCH being X-linked semi-dominant, rather than dominant as classified by OMIM.

CASK protein-domain organization shows a high degree of phylogenetic conservation among animals, even with a simple nervous system [31, 82]. According to DIOPT v.9 ([https://www.flyrnai.org/cgi-bin/DRSC\\_orthologs.pl](https://www.flyrnai.org/cgi-bin/DRSC_orthologs.pl), last accessed 14 June 2023), which integrates data from numerous orthology-prediction algorithms [61], *Drosophila melanogaster* CASK and human CASK are mutually orthologous. Reduction or absence of *Drosophila* CASK caused deficits of several types of associative learning or memory [48, 95]. In a striking example of conserved function, human CASK<sup>+</sup> can rescue defective CaMKII autophosphorylation in *Drosophila* CASK-LOF mutants [48]. Several animal models of CASK disorders are available; each has distinct strengths and weaknesses vis-a-vis construct and face validity. Brain size was reduced in some mouse LOF models and recurrent seizures were seen in others [85, 145]. Reduced expression of zebrafish CASK caused microcephaly and provided an assay to assess functional changes of human mutations [24]. Here we report the novel findings that a partial-LOF allele of *Drosophila* CASK reduces the size of both brain and neurite arbors of cultured neurons.

Given the sensitivity of human brain development to CASK-function level, neonates with CASK-related disorders could benefit from treatments that boost CASK function or ameliorate downstream consequences of the mutation. A needed step toward that goal is assay development for drug discovery. Using a partial-LOF CASK mutation, we developed a *Drosophila* model of mild-to-moderate CASK-related disorders with microcephaly that also provides a cell-based assay for phenotypic analysis and screening. Moreover, the network relationships between CASK and genes encoding its partners (Additional file: Table A1) suggest therapeutic strategies for a whole set of monogenic disorders.

In the past decade, microfluidic systems and technology have advanced to enable single-cell neuronal analyses [51] and drug screening using a variety of cell-based assays [28, 166]. A major bottleneck remains the dissociation of viable neurons from brain tissue. We developed microfluidic technology for standardized, automated brain tissue dissociation in which the CASK-mutant

neuronal phenotype is retained with high fidelity. These advances will enable compound screening of primary cultured neurons as a stepping stone toward therapeutic development.

## Methods

### Amino acid sequence comparison

We compared *Homo sapiens* CASK isoform 1 (NCBI Reference Sequence NP\_003679.2) to *Drosophila melanogaster* CASK isoform H (NCBI Reference Sequence NP\_001262811.1) using the BLOSUM62 similarity matrix [58] and the EMBL-European Bioinformatics Institute (EBI) tools collection (<https://www.ebi.ac.uk/Tools/>, last accessed 25 February 2022). The conserved protein-domain boundaries were based on HMMER's HMMSCAN and their pairwise sequence identities and similarities determined by EMBOSS program Needle. The dot-matrix display of amino acid similarity was generated by EMBOSS program Dotmatcher [94] using a Needleman-Wunsch global alignment. The settings selected were window length of 10 amino acids and score threshold of 30, which is somewhat more stringent than the default threshold of 23.

### *Drosophila melanogaster* genetic reagents and crosses

Fly stocks were maintained at room temperature (21–23 °C) on a masa corn flour-nutritional yeast-agar medium [37] supplemented with active baker's yeast. Cultures for experiments were reared at optimal larval density under standard conditions of 25 °C, 60–80% relative humidity, as described previously [74]. Stocks of X-ray-induced third-chromosome deficiencies, *Df(3R)X307* and *Df(3R)X313* (FlyBase ID FBal0048070 and FBal0048071, respectively; Fig. 1b), were obtained from the Bloomington *Drosophila* Stock Center (Bloomington, IN), and maintained over the balancer *TM6B, Tb e*. Based on low-resolution mapping [96], *Df(3R)X307* is the smaller deletion with breakpoints within the gene, removing most of CASK. *Df(3R)X313*, deletes most of CASK and additional downstream sequences, with an unknown left-hand breakpoint. Each deficiency is homozygous lethal during embryonic development, but neither recessive lethal has been mapped.

Three CASK stocks (Fig. 1c, d) were gifts from Dr. Leslie Griffith (Brandeis University, Waltham, MA): (i) the hypomorphic allele,  $\Delta I8$  (also known as *P18*), (ii) a precise-excision control allele, *Ex33* (also known as *Con*; [142], and (iii) a second-chromosome-insertion line of *UAS-CASK<sup>+</sup> 10.20* [32] generated in the laboratory of Dr. Peter Bryant (University of California—Irvine).  $\Delta I8$  was derived by imprecision excision of P-element EY07081 (Fig. 1b) from the first intron of CASK, 1751 bp upstream



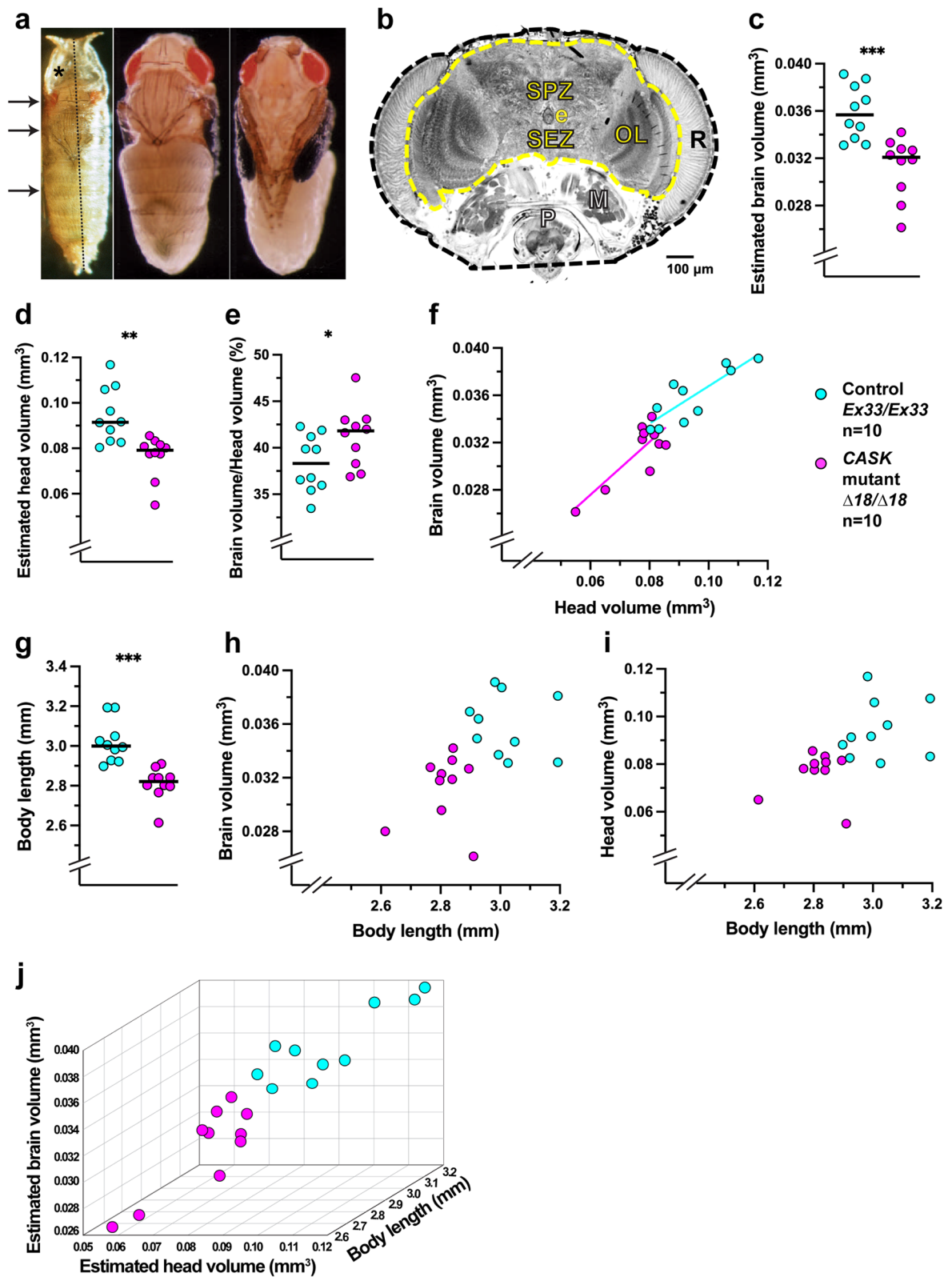


**Fig. 2** (See legend on previous page.)

The pupal cuticle, a transparent, thin membrane that shrink-wraps the developing fly, was removed from around the head. Using one tip of fine forceps as a blade (Dumont #5, Dumoxel with Biologie tips; Fine Science Tools, Inc., Foster City, CA, USA), the head was severed from the body and the distal proboscis removed. The latter step provides an entry point for reagents, enhancing fixation and embedding of internal soft tissues.

#### **Fixation and embedding**

Each head was processed individually. The protocol was modified from one used for estimating brain volumes of larger insects [130]. Unless otherwise stated, chemicals were purchased from Electron Microscopy Sciences (Hatfield, PA, USA). Heads were fixed overnight in freshly diluted 4% formaldehyde in PBS, pH 7.4, at 4 °C on a platform rocker (Roto-Shake Genie, Scientific Industries, Bohemia, NY, USA). Unless otherwise stated, all subsequent steps were at room temperature. After fixation, each head was transferred to a microcentrifuge tube and washed twice in PBS, pH 7.4, for 1 h each, and in distilled water for 1 h. Washes and subsequent steps were done on the platform rocker. To stain the tissue, the heads were incubated in osmium tetroxide, 1% in H<sub>2</sub>O, for 2 h at 4 °C and an additional hour at room temperature, then rinsed in water for 3 h. A one-step dehydration method [23, 36] was performed by placing samples in 2,2-dimethoxypropane (TCI America, Portland OR, USA), acidified to ~0.03% v/v hydrochloric acid, for 15 min. After dehydration, heads were first immersed in 100% acetone for 20 min, then transferred to 30% acetone/70% Spurr low-viscosity embedding resin for 6 h, and finally into 100% resin overnight. Each specimen was mounted in a BEEM™ (VWR) embedding capsule filled with 100% Spurr resin, and oriented for sectioning in the frontal plane; occasionally, the head would tilt before the resin solidified. Resin polymerization was induced by overnight incubation at 70 °C.

#### **Serial sectioning**

Each polymerized block was secured in a specimen holder and trimmed into a rectangle around the head using a disposable single-edge razor blade. Serial sections, 12 µm, were cut on a sliding microtome (Reichert, Austria) with a stainless-steel knife. Serial sections of each head were arranged using a moist paintbrush in rows on a single microscope slide on a warming tray at 60 °C to facilitate flattening. Section recovery was >99%; lost sections were documented. The slides were mounted with Cytoseal (Thermo Scientific™, Waltham, MA) and coverslipped. These are permanent preparations.

#### **Image acquisition and analysis**

Digital images of each histological section (Fig. 2b) were acquired with an Olympus DP70® camera mounted on an Olympus BX51TF® (Tokyo, Japan) compound microscope, using a 20X objective (numerical aperture, 0.50). For any section that was not flat, several images were acquired at different focal planes, merged using Adobe Photoshop (Adobe Systems Inc., San Jose, CA), and adjusted for brightness and contrast. To estimate volumes from serial sections, Olympus cellSens™ Entry software (v.1.14) was used to quantify the area of anatomical structures. Outlines of the head perimeter and of the CNS therein (“brain”) were traced using the *measure polygon* tool, which provides the number of pixels within the outlined area. To approximate the volume contributed by the proboscis, the ventral margin of the head was drawn across the midline, connecting the right and left ventral-most points (Fig. 2b). In sections with non-contiguous CNS tissue, several polygons were outlined and measured. A stage micrometer (Ward’s Science, Rochester, NY, USA) was used for calibration. In the case of one lost section, the values of its head and brain areas were assumed to be midway between those of the flanking sections. Several sections (<0.5%) were partly folded, obscuring one side of the head/brain; this was estimated from the area of the contralateral side. The summed areas of all sections of each sample were multiplied by section thickness (12 µm) to estimate head and brain volumes.

#### **Primary neuronal cultures from developing CNS tissue**

Dissociated neuronal cultures were prepared from the whole CNS of w3L as previously described [74, 75, 143]. At this stage of development, CNS cells include mature neurons, incompletely differentiated neurons, glia, and neural stem cells. For comparison among genotypes, larvae were matched for sex and culture density. Cell-culture medium was prepared using two fetal bovine serum (FBS) sources at different times. Most experiments used FBS from Hyclone (Logan, UT; lots APC20860 or AZA180873), while a few used Optima FBS (Atlanta, GA; lot #D0118); Hyclone FBS supported better neurite outgrowth. After incubation in enzymes that digest the extracellular matrix, the CNS was dissociated either by manual trituration [143] or in a microfluidic device (see below). Both methods generate suspensions of viable neurons and neural stem cells. Dissociation severs all axonal and dendritic extensions from neurons, which re-elaborate arbors during in vitro culture. Neural stem cells proliferate for at least one day in vitro (div; data not shown); their progeny neurons then differentiate de novo.

Each CNS-cell suspension was plated by distributing it into five or six custom culture dishes [143], either made in-house or purchased from MatTek (Ashland, MA).

After 2–3 h at 25 °C to allow the cells to adhere to the substrate, the dishes were flooded with culture medium and maintained at 25 °C for 3 div (~70–80 h post-plating). Neurite outgrowth starts within hours, and a complex neurite arbor can be seen at 3 div [74, 143]. Overlap between neighboring arbors is usually limited, allowing evaluation of individual neurons. Data acquisition and analyses were 'blinded' by having dishes coded for preparation method and genotype by a lab member not involved with that experiment.

Rat and mouse E18 hippocampi were purchased from BrainBits® (Springfield, IL, USA; now Transnetyx Tissue) which ships tissue in a proprietary physiological stabilization solution, Hibernate® EB (HEB), along with supplies for neuronal culture. Each hippocampus was cut into four pieces with iridectomy scissors. The pieces were transferred in a sterile 9" Pasteur pipette with minimal HEB medium into freshly-made papain (2 mg/ml in Hibernate® E without calcium or B27®). The tissue was digested for 10 min at 30 °C, with gently swirling every 2 min. Following digestion, the tissue was transferred to fresh HEB at room temperature for 5–10 min. prior to loading each piece into a microfluidic device for dissociation. The recovered cells were sedimented by brief centrifugation, washed in NbActiv1® plus glutamate (Neurobasal® + B27® + Glutamax®), and plated on glass coverslips coated with poly-D-lysine. The cells were flooded with the same medium and cultured for 4–5 div at 37 °C with 5% v/v CO<sub>2</sub>.

### Neurite-arbor size and shape analysis

Fixation for immunostaining of cultured neurons was performed as described previously [74, 76, 143]. The neuronal membrane protein Nervana 2 [146] was labeled with polyclonal goat anti-horseradish peroxidase (anti-HRP) (Sigma, St. Louis, MO) at 1:500, detected by Donkey anti-Goat IgG Alexa Fluor® 488 or Donkey anti-Goat IgG Alexa Fluor® 568, both from Molecular Probes (Life Technologies), diluted 1:500. Nervana 2's high abundance and uniform distribution provide a strong, contiguous signal along the neurite as it tapers to a fine tip. Stained cultures were mounted under a coverslip in 12% w/v polyvinyl alcohol (Sigma, St. Louis, MO) with 1.5% w/v DABCO (1,4-diazabicyclo [2.2.2] octane; Sigma), an anti-fading reagent, and stored at 4 °C in the dark.

Neuronal nuclei were identified with anti-ELAV mouse monoclonal antibody, mAb5D3C5 [132, 144] at 1:100, detected by Goat anti-Mouse Cy3 (Jackson ImmunoResearch, West Grove, PA, USA) at 1:400. To identify glia expressing the *repo-lacZ* reporter, we used pre-absorbed rabbit polyclonal anti- $\beta$ -galactosidase ( $\beta$  gal) (Cappel, Malvern, PA, USA) at 1:50 as described [76] and Goat

anti-Rabbit Alexa Fluor® 488 (Molecular Probes, Life Technologies) at 1:300. This strategy allowed neurons and glia to be labeled in the same cultures. To detect GAL4-driven GFP expression by immunostaining, chicken anti-GFP IgG (Life Technologies) was used with Goat anti-Chicken IgG Alexa Fluor® 488 (Molecular Probes), both at 1:500.

Live and immunostained cultured *Drosophila* neurons were examined on a Diaphot 300 inverted microscope (Nikon, Tokyo, Japan), with 40X (numerical aperture, 1.0) or 60X oil-immersion (numerical aperture, 1.4) objectives, using phase-contrast and fluorescence optics. Fluorescent signal was detected with filter cube Chroma #41001 (exciter 460–500 nm; dichroic 505 nm; bandpass emitter, 510–560 nm) for Alexa Fluor® 488 and with Nikon G-2A filter cube (exciter, 510–560 nm; dichroic 580 nm; long-pass emitter, 590 nm) for Alexa Fluor® 568 and Cy3. Images were acquired with Hamamatsu ORCA-285 digital camera (Hamamatsu Photonic Systems, Bridgewater, NJ, USA) and HCLImage® software (v.2.0.0.0; Hamamatsu). Hippocampal neurons were viewed at 10X, 20X, or 40X under phase-contrast.

For quantitative analysis of neurite arbors, a systematic sample of ~100 neurons (i.e., cell body and complete neurite arbor) was imaged from a single culture dish, using the staircase-sampling method [143]. Neurons with modest overlap of neighboring arbors were also included. Exclusion criteria for imaging a neuron included weak anti-HRP signal (suggesting cell death), damaged cell bodies, and overlapping arbors that could not be resolved to allow accurate image analysis. For neurons with larger arbors extending beyond the 60X microscopic field, multiple overlapping images were acquired and merged by "stitching", using PanaVue ImageAssembler® software (Panavue Inc., Québec, Canada).

Digital images were converted from 16-bit to 8-bit tiff for analysis by semi-automated custom software, NeuronMetrics™ [115, 143], which converts each neurite arbor into a one-pixel-wide skeleton connected to the cell body and bounded by the neuron's convex polygon ("territory"). Two key features of NeuronMetrics™ are algorithms that (i) connect gaps in the skeleton (due to variation in fluorescence intensity) and (ii) correct branch numbers for neurite-to-neurite contacts within the same arbor. NeuronMetrics™ computes number of primary processes (also called primary neurites), neurite-arbor total neurite length, branch-number estimate, territory area, and territory perimeter. From these, additional measures were calculated: higher-order branch number (total branches minus primary neurites), branch density (branches per 1000  $\mu$ m<sup>2</sup> territory area), and branches per unit length. After statistical analysis, the code was broken.

### Microfluidic systems for brain-tissue dissociation

The microfluidic system includes several components: (1) a transparent microdevice with one or more parallel channels; (2) an external fluid-handling system (including a programmable syringe pump, a pressure transducer, a valve, inlet/outlet connectors, and tubing); (3) a microscope and camera for real-time monitoring and image acquisition; and (4) a computer connected to both the pump and microscope. Microdevice design and fabrication were similar to those previously described [68] with numerous design variations tested for optimization. Single- and dual-microchannel devices were fabricated from molded polydimethylsiloxane (PDMS; Sylgard 184 silicon elastomer, Dow Corning, USA) using standard micro-fabrication techniques. In brief, a computer numerical control (CNC) machine was used to create reusable aluminum molds with the designed microchannel patterns. A mixture of PDMS base and curing agent was poured into the mold(s) and polymerized at 50 °C. After peeling off the cured PDMS sheet from the mold, holes were punched at each end of the channel groove for the inlet/outlet ports. The device fabrication process was completed by bonding the molded PDMS substrate to a flat PDMS substrate following oxygen plasma treatment. The inner surfaces of the formed PDMS channel were highly hydrophobic preventing adhesion of tissue or neurons during experimentation. These methods are well-established to be biocompatible [141].

The overall channel length was ~40 mm with a mirror-image symmetric design. Each channel was 2 mm wide at its distal ends, gradually tapering to 1 mm approaching the center. Tissue dissociation, driven by oscillatory fluid flow, took place in the narrow central orifice flanked by the two wider segments. The side walls in the transition zone between the wider channel segments and the orifice form ~45-degree angles symmetric with respect to the channel central axis. For sterilization, the channels were flushed with 70% ethanol prior to connecting them to the pump, followed by device treatment under UV light. Because PDMS is elastic, the device was sandwiched between two rigid acrylic plates during the dissociation experiment to keep the orifice dimensions fixed under high pressure.

Fluid flow was driven by an Infuse/Withdraw PHD ULTRA syringe pump (Harvard Apparatus, Holliston, MA, USA) controlled by a custom-designed interface in LabVIEW (National Instruments, 2015, USA) running on a standard desktop computer with Windows operating system. The tubing connecting the pump to the microdevice had internal diameter 1/16 inch. The system was primed with fresh culture medium prior to sample loading. Enzyme-treated brain tissue (fruit fly or rodent) in fresh culture medium was loaded manually with a

micropipette (Gilson, Middleton, WI, USA) and positioned adjacent to the central orifice under direct microscopic observation. Numerous combinations of fluid-flow parameters (infusion volume, oscillation frequency, flow rate and cycle number) were tested for each tissue type, with most assessments by holistic scoring (excellent, very good, good, fair, poor).

### Statistics and graphing

Pair-wise comparisons of individual parameters between genotypes were made using the non-parametric Mann–Whitney rank sum test for non-normally-distributed data [40]. The tests were implemented in RStudio (RStudio 2022.07.2 + 576 "Spotted Wakerobin" Release, R version 4.2.2 GUI 1.79 High Sierra build; R Core Team, 2022) under the GNU General Public License, using scripts developed by J.A.T. Graphs were created using R scripts or GraphPad Prism (version 9.0.0 for Mac, GraphPad Software, San Diego, CA, USA). Photomicrographs of immunostained neurons underwent cropping and "Autocontrast" adjustment in Adobe Photoshop. Figures were assembled and edited using Adobe Illustrator version 26.4.1 (Adobe, Inc., San Jose, CA, USA).

Comparisons of *Δ18* and *Ex33* homozygotes performed over several years were analyzed using a linear mixed effects model. This allows use of data across multiple repeated studies with inter-experiment variability, e.g., due to differences in reagents and environments. For each neurite-arbor parameter, each experiment represents a single sample with a summary statistic, the median. The method first calculates the genotype-to-genotype median difference within each experiment, the mean of the median differences across all experiments, standard error of the mean, and 95% confidence interval. The mixed effects model fits a random intercept for each experiment (medians) and genotype fixed effects within an experiment. For each parameter, the differences between genotypes are subjected to a two-tailed t test. The analysis was implemented in the R package nlme using the lme function (version 3.1–160; [127]).

## Results

### *A Drosophila CASK-LOF mutation causes microcephaly, microencephaly, and a form of short stature*

We found that, despite 700 million years of evolutionary distance from a common ancestor, human and fruit fly CASK show remarkable phylogenetic conservation (Fig. 1a; Additional file: Fig. A14). The functional domains of *Drosophila* CASK have 52–87% amino-acid similarity to those of human CASK, with the highest in the PDZ and GUK domains (87% for both) and lowest in the L27 domains. Human CASK mutations cause microcephaly

and short stature, which co-occur in a subset of monogenic neurodevelopmental disorders with intellectual disability [14]. We used the partial-LOF *CASK* mutation (Fig. 1c) to determine whether *Drosophila CASK* controls brain size and body length, comparing  $\Delta 18$  homozygous mutants with *Ex33* homozygous controls.

*CASK*-mutant  $\Delta 18$  homozygous flies do not have obvious malformations of either head or brain development. For brain- and head-volume estimates, we analyzed serial histological sections of fly heads at the end of metamorphosis (Fig. 2b), when brain morphology is mature at the light-microscopic level. We are using "brain" to mean all CNS tissue in the head – the cerebral and gnathal ganglia, also called supra- and subesophageal zones [66], this includes structures functionally analogous to the brain and brainstem of mammals. *CASK*-mutant flies had significantly smaller brains compared to genetic controls ( $p < 0.001$ ; Fig. 2c). Thus, the *CASK*-mutants have microencephaly. *CASK* mutants also have smaller heads than their genetic controls ( $p < 0.001$ ; Fig. 2d); in other words, *CASK*-LOF mutants have microcephaly. This was somewhat surprising because, while mammalian head growth is mechanically driven by brain growth, the two processes are anatomically separate during *Drosophila* development [43]. Quantification of the percentage of head volume occupied by the brain, showed that *CASK*-mutant brains occupied a slightly but significantly greater fraction of the head ( $p < 0.05$ ) compared to genetic controls (Fig. 2e). This suggests that the reduction in head size of *CASK*-mutant flies is somewhat more severe than their reduced brain size. The positive linear relationship between brain and head volumes (Fig. 2f) seen in controls is retained in the mutants, with a shift in data distribution to lower values but no significant difference in slopes derived from linear regression analysis. (Controls:  $y = 0.159x + 0.021$ ;  $R^2 = 0.71$ . Mutants:  $y = 0.224x + 0.014$ ;  $R^2 = 0.67$ ).

We measured body length (head-thorax-abdomen) along the longitudinal axis of the protective cocoon-like puparium (Fig. 2a) which forms from the larval cuticle at the start of metamorphosis. It directly reflects larval length, which dictates the length of the adult. It is stable, stationery, and firm, hence easy to measure. In comparative anatomy terms, insect-puparium length is most similar to mammalian crown-rump length (CRL), a commonly used measure of fetal growth in humans and other vertebrates [77, 123]. *CASK*  $\Delta 18/\Delta 18$  mutants have significantly shorter body length than *CASK Ex33/Ex33* controls ( $p < 0.0005$ ) (Fig. 2g). Thus, like the human orthologue, *Drosophila CASK* promotes growth along the longitudinal body axis. This is also consistent with an average ~15% reduction in body weight of  $\Delta 18/\Delta 18$  compared with *Ex33/Ex33* [42].

When brain and head volumes were compared with body length, the relationships do not appear linear for either genotype (Figs. 2h, i, respectively). This suggests that the reduced brain and head volumes of *CASK* mutants are not simply a consequence of reduced animal size. In a 3D scatter plot of body length, head volume, and brain volume (Fig. 2j), the data from mutants and controls form two non-overlapping groups. In summary, *Drosophila CASK* is required for the developmental attainment of normal brain volume, head volume, and body length.

### **CASK LOF disrupts neurite-arbor morphogenesis: the bushy phenotype**

The abnormally small brains of *CASK*-mutant adults raise the question of when during development this size deficit arises. In mature larvae (w3L), freshly explanted CNS of *CASK* mutants ( $\Delta 18/\Delta 18$ ) were visibly smaller than those of controls (*Ex33/Ex33*) of the same sex and developmental stage (Fig. 3a). Hence, microencephaly predates the onset of metamorphosis. Nonetheless, cellular densities after CNS dissociation and plating, as well as

(See figure on next page.)

**Fig. 3** The "bushy" phenotype of *CASK*-mutant neurite arbors in vitro. **a** The *CASK*-mutant larval CNS is reduced in size. Stereomicroscopic view of freshly dissected, unfixed whole-CNS explants from wandering third-instar female larvae in buffered saline, dorsal side up, anterior to the top. *CASK* control (*Ex33/Ex33*; left) alongside mutant ( $\Delta 18/\Delta 18$ ; right). OL, optic lobe; Br, brain; \*, subesophageal zone; VG, ventral ganglia; pn, peripheral nerves. Scale bar = 100  $\mu$ m. **b-h** Photomicrographs of cultured larval CNS neuron, immunofluorescently labeled for a neuronal membrane marker, after 3 div (60X magnification). **b** NeuronMetrics software output. The color-coded lines have been thickened to improve visibility: yellow polygon, territory; blue, central portion of the neuronal cell body; green, branches of the skeletonized neurite arbor. Scale bar = 10  $\mu$ m. **c-h** Scale bar = 20  $\mu$ m. Neurons representing the ~25<sup>th</sup> (**c, f**), ~50<sup>th</sup> (**d, g**), and ~75<sup>th</sup> (**e, h**) percentiles for each of three arbor-size parameters, total neurite length, territory area, and branch density. **c-e** *CASK* control, *Ex33/Ex33*. **f-h** *CASK* mutant,  $\Delta 18/\Delta 18$ . **(i-l)** The "bushy" phenotype: *CASK*-mutant neurite arbors are reduced in size with excessive branch density. Quantification of neurite-arbor morphology, depicted as box-plot distributions, comparing 3 div cultures of *CASK*-control (*Ex33/Ex33*;  $n = 106$  neurons; aqua) and *CASK*-mutant ( $\Delta 18/\Delta 18$ ;  $n = 105$  neurons; magenta) larval CNS neurons. Center lines and arrowheads represent the 50<sup>th</sup> percentile. Top and bottom of each box represent the 75<sup>th</sup> and 25<sup>th</sup> percentiles, respectively. The upper and lower whiskers represent the 90<sup>th</sup> and 10<sup>th</sup> percentiles, respectively. Significance levels: \*\*\*,  $p < 0.0005$ ; \*\*\*\*,  $p < 0.00005$ . Total neurite length (**i**), territory area (**j**), and higher-order branch number (**k**) were all reduced in *CASK*-mutant neurons, whereas branch density (**l**) was increased. These data are from one of 9 independent experiments; see Additional file: Table A3 for analysis across all experiments

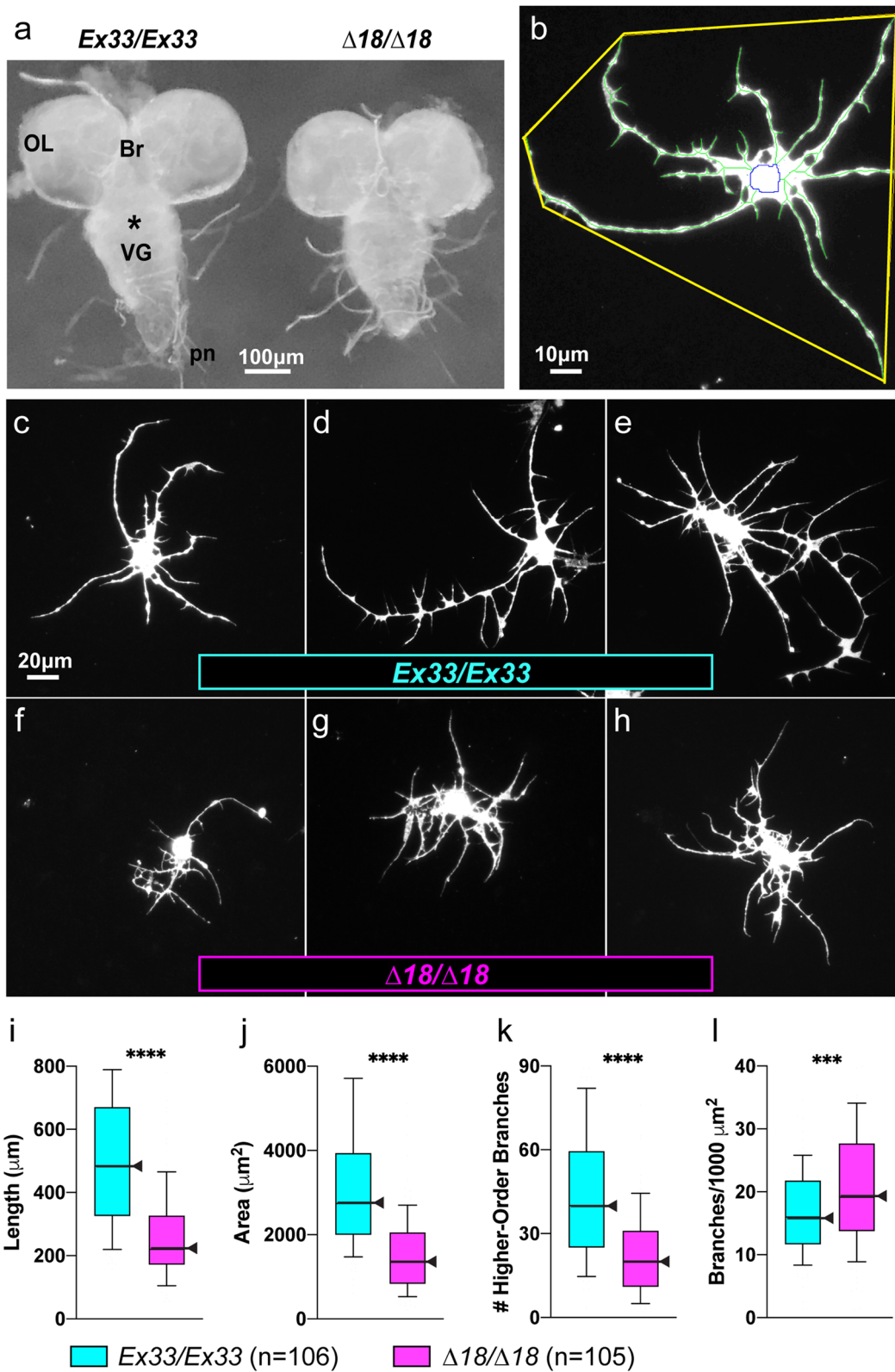


**Fig. 3** (See legend on previous page.)

after culture for 3 div, did not differ between the two genotypes by holistic microscopic examination by an expert practitioner (J.A.T.;  $n=9$  independent experiments).

Unlike neuronal density, neurite arbors of *CASK*-mutant cultured neurons were obviously smaller after 3 div from those of controls. Qualitatively, the mutant arbors appeared “bushy”: relatively small and more compact (Fig. 3c-h). To quantify neurite-arbor morphogenesis in vitro, we compared primary cultures prepared from the entire CNS of *CASK*-mutant ( $\Delta 18/\Delta 18$ ) and control (*Ex33/Ex33*) w3L using NeuronMetrics™ software to analyze digital images of immunofluorescently stained neurons sampled from each culture. (Fig. 3b; [115, 143]. For *CASK*-mutant arbors, total neurite length (Fig. 3i) and territory area (Fig. 3j) were reduced whereas branch density was elevated (Fig. 3l), all three with high degrees of statistical significance. Total branch and higher-order branch numbers (Fig. 3k) were reduced in most experiments. Primary process numbers were not significantly different between genotypes, suggesting that initiation of neurite outgrowth from *CASK*-mutant neuronal somata was not altered. The bushy phenotype is a population phenomenon, recognizable by microscopic inspection of individual dishes of cultured neurons. For single neurons, the differences from control are most apparent when comparing cells from approximately the same percentile of their distributions (e.g., Fig. 3c and f; d and g; e and h).

Because the entire CNS is dissociated, the cultures include diverse neuronal types with distinct in vivo morphologies (e.g., [67, 72, 136]. Histograms of neurite-arbor parameter distributions were unimodal for both *CASK* mutants and controls (Additional file: Fig. A2). This suggests that the bushy neurite-arbor defect is widespread rather than restricted to a small subset(s) of neurons, which would be consistent with the widespread *CASK* expression throughout the developing *Drosophila* CNS [32, 92, 96].

Quantitative data were obtained from nine pairwise comparisons ( $\Delta 18/\Delta 18$  vs. *Ex33/Ex33*) conducted over a period of several years with different laboratory locations, culture dishes, and biological reagents used (notably FBS). In addition, while most CNS dissociations were performed by manual trituration, some took place within microfluidic devices in a third location. As previously observed [76], there was considerable variation in the absolute values of morphometric parameters across experiments (e.g., Figs. 3i-l and 4a-h). For example, median total neurite length of control (*Ex33/Ex33*) arbors ranged from 305  $\mu\text{m}$  to 652  $\mu\text{m}$ . Nonetheless, the differences between genotypes were very consistent. For statistical analysis of data from all nine experiments, we used a linear mixed effects model in which each experimental median is considered a single sample (Additional

file: Table A3). The differences between *CASK*-mutant and control neurite arbors were highly significant statistically, with magnitudes suggestive of biological significance: total neurite length (-35%;  $p=0.0008$ ), territory area (-48%;  $p=0.0004$ ), higher-order branch number (-30%;  $p=0.0023$ ) and branch density (+39%;  $p=0.0006$ ). Thus, the bushy phenotype of *CASK*-mutant neurite arbors represents a robust biological deviation from wild-type morphogenesis in vitro.

### The bushy phenotype is sensitive to *CASK* dosage

Human females with *CASK*-related disorders have semi-dominant mutations with strong evidence of haploinsufficiency and other indicators of dosage sensitivity (e.g., [57]. To explore potential genetic parallels between *CASK* in fly and human, we compared neurite arbors of three genotypes: homozygous control (*Ex33/Ex33*), homozygous hypomorphic mutant ( $\Delta 18/\Delta 18$ ), and heterozygous ( $\Delta 18/Ex33$ ). When a phenotype is strictly recessive, homozygous controls and heterozygotes consistently have the same (wild-type) characteristics; when a phenotype is strictly dominant, homozygous mutants and heterozygotes consistently have the same abnormal manifestations. In independent replicate experiments, we observed that  $\Delta 18/Ex33$  larval neurons grew arbors with median parameters between those of  $\Delta 18/\Delta 18$  and *Ex33/Ex33* homozygotes (Fig. 4a-h). In the statistical analyses, territory area (Fig. 4b, f) and branch density (Fig. 4d, h) values of  $\Delta 18/Ex33$  neurons were significantly different from both homozygotes in one experiment (Fig. 4f, h) but not significantly different from  $\Delta 18/\Delta 18$  mutants in the other experiment (Fig. 4b, d). Total neurite length of  $\Delta 18/Ex33$  was either not different from  $\Delta 18/\Delta 18$  mutant (Fig. 4a) or not different from *Ex33/Ex33* control (Fig. 4e). Thus, the features of the core triad of bushy neurite-arbors – decreased total length, decreased territory area, and increased branch density – do not behave like strictly recessive or dominant phenotypes. Rather these data suggest semidominance. In contrast, higher-order branch numbers, which across many experiments were less consistently reduced in  $\Delta 18/\Delta 18$  mutant neurite arbors, were not significantly different between *Ex33/Ex33* control and  $\Delta 18/Ex33$  neurons (Fig. 4c, g), suggesting this phenotype may be recessive.

To clarify the effects of *CASK*-gene dosage, we used two chromosomal deletions that remove all *CASK* function, *Df(3R)X307* and *Df(3R)X313*. With no *CASK*-null allele available, these are particularly valuable tools (Fig. 1b). Flies with compound heterozygous deletions [*Df(3R)X307/Df(3R)X313*] are viable as adults and sometimes called “*Caki* mutants” [96, 142]. Thus, unlike in humans and mice, *Drosophila CASK* is not essential for organismal viability. We used each deficiency chromosome to

reduce *CASK* function beyond that in  $\Delta 18/\Delta 18$ , assessing neuronal phenotypes of  $\Delta 18$  hemizygotes,  $\Delta 18/Df(3R)$ . Because  $\Delta 18$  is hypomorphic, we predicted the bushy phenotype would become more severe. For each deletion, we compared three genotypes (e.g., Fig. 5a-c):

- 1) hemizygous control:  $w/+$  or  $w/w; +; Ex33/Df(3R)$
- 2) homozygous mutant:  $w/w; +; \Delta 18/\Delta 18$
- 3) hemizygous mutant:  $w/w; +; \Delta 18/Df(3R)$

For both deficiencies, arbors of hemizygous mutant neurons showed highly significantly reduced total neurite length, territory area, and higher-order branch number, along with increased branch density compared with hemizygous controls (Fig. 5d-k). Moreover, hemizygous mutant neurons were at least as severely affected as homozygous  $\Delta 18$  mutant neurons. For both deficiencies, this was most evident for total neurite length and territory area, which were significantly smaller in  $\Delta 18/Df(3R)$  than in  $\Delta 18/\Delta 18$  (Fig. 5d-e, h-i). Hence, the bushy phenotype shows a severity range inversely related to *CASK*-gene dosage (in decreasing order of phenotypic severity):  $\Delta 18/Df(3R) > \Delta 18/\Delta 18 > Ex33/\Delta 18 > Ex33/Ex33$ .

### Transgenic *CASK*<sup>+</sup> improves the bushy phenotype

A definitive method for proving a phenotype is due to LOF of a specific gene is to demonstrate rescue by a wild-type transgene. We therefore tested whether wild-type *CASK* would rescue neurite-arbor size and shape in  $\Delta 18$  homozygotes. The degree of rescue may depend on the nature of the mutation and the genetic reagents used. We used *elav-GAL4*<sup>C155</sup> to drive expression in neurons of a single-copy transgene, *UAS-CASK*<sup>+</sup>, a cDNA encoding full-length wild-type *CASK*. For two reasons, we expected that rescue might be strong but incomplete. First, the phenotype is dosage-sensitive (Figs. 4 and 5). Second, *elav-GAL4*<sup>C155</sup> drives expression in a large majority of cultured neurons (~85%; see Methods), but is not fully pan-neuronal in vitro. Hence, we predicted that one transgenic copy of *CASK*<sup>+</sup> would provide partial restoration of *CASK* function and yield an intermediate phenotype, better than that of  $\Delta 18$  homozygotes, but not as good as control (*Ex33*) homozygotes.

We first tested whether either of the two transgenes would impact the bushy phenotype of *CASK*-mutant  $\Delta 18$  homozygotes. A three-way comparison was performed as follows:

- 1) homozygous mutant:  $w/w; +; \Delta 18/\Delta 18$
- 2) driver transgene in mutant background: *elav-Gal4*<sup>C155</sup>  $w/w; +; \Delta 18/\Delta 18$

- 3) target transgene in mutant background:  $w/+; UAS-CASK^+/+; \Delta 18/\Delta 18$

Neither of the two transgenes improved the neurite-arbor phenotype of *CASK*  $\Delta 18$  homozygous mutants (Fig. 6a-d). In fact, both transgenes caused modest worsening, i.e., reductions in neurite-arbor size beyond that of homozygous mutant neurons. Total length was significantly reduced by both *UAS-CASK*<sup>+</sup> and *elav-GAL4*<sup>C155</sup>; territory area by *UAS-CASK*<sup>+</sup> only. Either or both of these effects could make detection of phenotypic rescue more difficult, at least for arbor size. Neither transgene affected branch density (one of the most characteristic features of the bushy phenotype) or higher-order branch number.

To test for transgenic rescue of the bushy phenotype, three replicate experiments, performed in parallel to minimize biological and technical variables, compared neuronal cultures from three genotypes:

- 1) homozygous control:  $w/w; +; Ex33/Ex33$
- 2) homozygous mutant:  $w/w; +; \Delta 18/\Delta 18$
- 3) experimental: *elav-Gal4*<sup>C155</sup>  $w/+; UAS-CASK^+/+; \Delta 18/\Delta 18$

Expression of a single wild-type *CASK*<sup>+</sup> cDNA transgene in the large majority of  $\Delta 18$  homozygous mutant neurons resulted in highly significant increases in total neurite length, territory area, and higher-order branch number, along with decreases in branch density (Fig. 6e-h). In other words, the bushy phenotype was significantly improved, with neurite-arbor parameters intermediate between those of mutant and control homozygotes. This highly significant partial rescue is strong confirmatory evidence that the bushy phenotype maps to *CASK* and results from *CASK* LOF.

### Optimization of microfluidic technology for CNS tissue dissociation

The robust nature of the bushy phenotype, with visible and quantitative features, makes it a strong candidate for phenotype-based screening for drug discovery. We previously demonstrated that primary neuronal cultures can be screened for compounds that modify a neurite-arbor defect [75]. However, manual dissociation is a major obstacle because it is highly fatigable, non-trivial to learn, and uncontrolled in terms of shear stress applied to the tissue. In fact, the shear stress generated during manual trituration has never been estimated. The rate-limiting step of CNS tissue dissociation must be overcome before screening speed can be scaled up toward high throughput. Microfluidic technology has the potential to solve

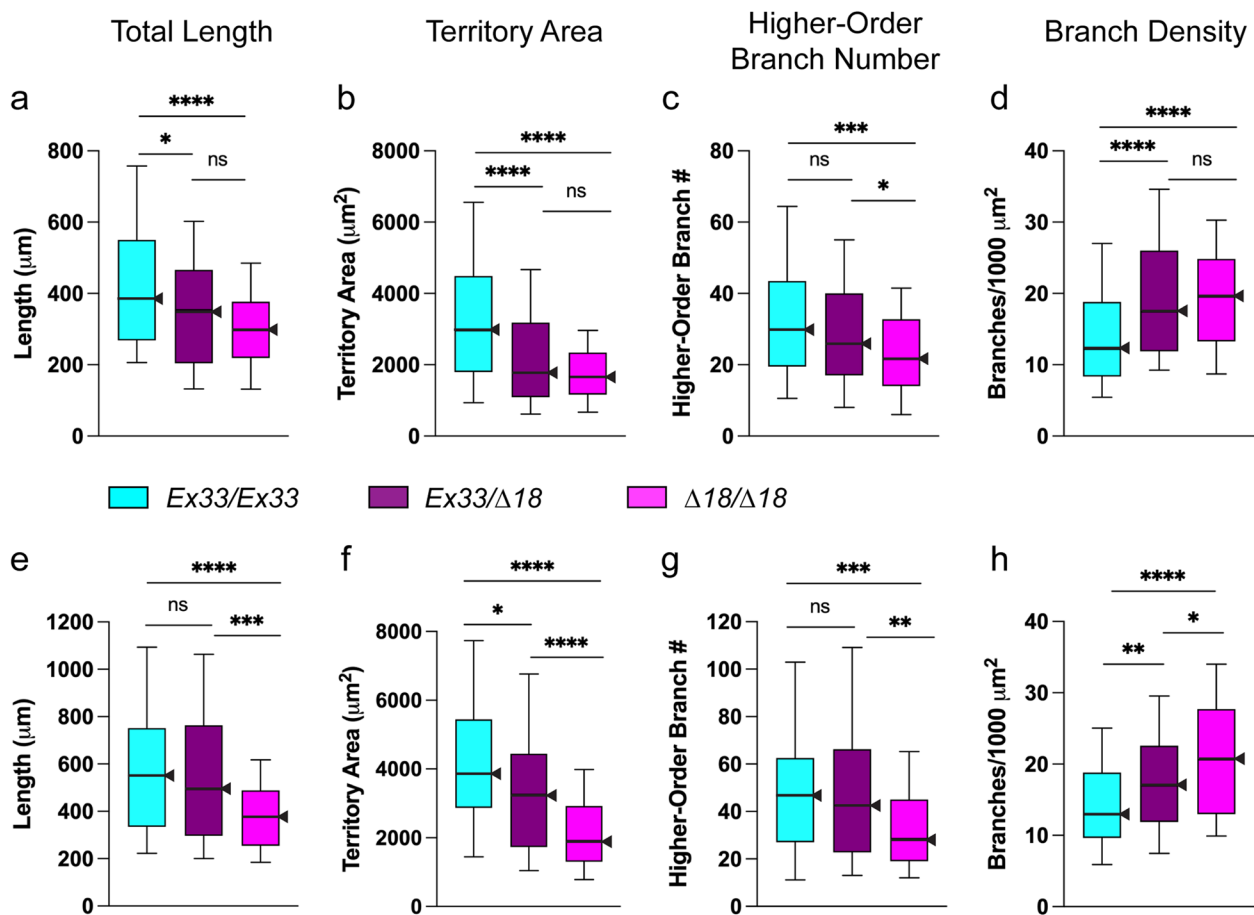


**Fig. 4** Analysis of  $\Delta 18$  heterozygous neurons shows the bushy phenotype is neither strictly recessive nor dominant. Data from two independent experiments (**a–d** and **e–h**, respectively), each with parallel 3-div cultures of larval CNS neurons from *CASK* control (*Ex33/Ex33*; aqua), *CASK* mutant ( $\Delta 18/\Delta 18$ ; magenta), and heterozygote ( $\Delta 18/Ex33$ ; burgundy). Box-plot distributions depicted as in Fig. 3, with  $n = 101–104$  neurons from each genotype in each experiment. **a, e** Total neurite length; **b, f** territory area; **c, g** higher-order branch number; and **d, h** branch density. For two key characteristic features of the bushy phenotype, decreased territory area and increased branch density,  $\Delta 18$  was dominant (**b, d**) or semi-dominant (**f, h**). Decreased total neurite length showed opposite results in the two experiments (**a, e**) and decreased higher-order branch number appeared to be recessive (**c, g**). Significance levels: \*,  $p < 0.05$ ; \*\*\*,  $p < 0.0005$ ; \*\*\*\*,  $p < 0.00005$

this problem. Manually dissociated cells from prenatal spinal cord were sorted within a microfluidic device prior to culture [162]. Several groups reported dissociation of non-neural-tissue into viable cells – rodent kidney, liver, heart, adipose tissue, and tumors, as well as human placenta and endometrium [3, 5, 93]. Relative to other cell

types, the unique structure of neurons adds a challenge – axons and dendrites are severed during dissociation and the neuronal membrane must reseal at each detachment point.

We previously reported initial success with development of a mechanized, observable, standardized – and

(See figure on next page.)

**Fig. 5** Chromosomal deficiencies of *CASK* reveal dosage sensitivity of the bushy phenotype. For two deficiencies, 3 div larval CNS cultured neurons were compared among three genotypes: *CASK* homozygous mutant ( $\Delta 18/\Delta 18$ ), *CASK* hemizygous mutant ( $\Delta 18/Df$ ), and control allele over deficiency (*Ex33/Df*). **a–c** Photomicrographs of representative neurons, immunostained for neuronal membrane marker, from near the median for each of three parameters: total neurite length, territory area and branch density. 60X magnification; scale bar = 20 μm. **a** *Ex33/Df(3R)X313*. **b–c** Both  $\Delta 18/\Delta 18$  and  $\Delta 18/Df(3R)X313$  neurons show bushy neurite arbors. **d–k** *CASK* hemizygous mutant neurons are more severely affected on most parameters. Quantification of neurite-arbor morphology; box-plot distributions depicted as in Fig. 3. Significance levels: \*,  $p < 0.05$ ; \*\*\*,  $p < 0.0005$ ; \*\*\*\*,  $p < 0.00005$ . **d–g** *Ex33/Df(3R)X307* ( $n = 104$ ; orange) compared with  $\Delta 18/\Delta 18$  ( $n = 106$ ; magenta) and  $\Delta 18/Df(3R)X307$  ( $n = 106$ ; green). **h–k** *Ex33/Df(3R)X313* ( $n = 106$ ; orange), compared with  $\Delta 18/\Delta 18$  ( $n = 105$ ; magenta) and  $\Delta 18/Df(3R)X313$  ( $n = 106$ ; green)

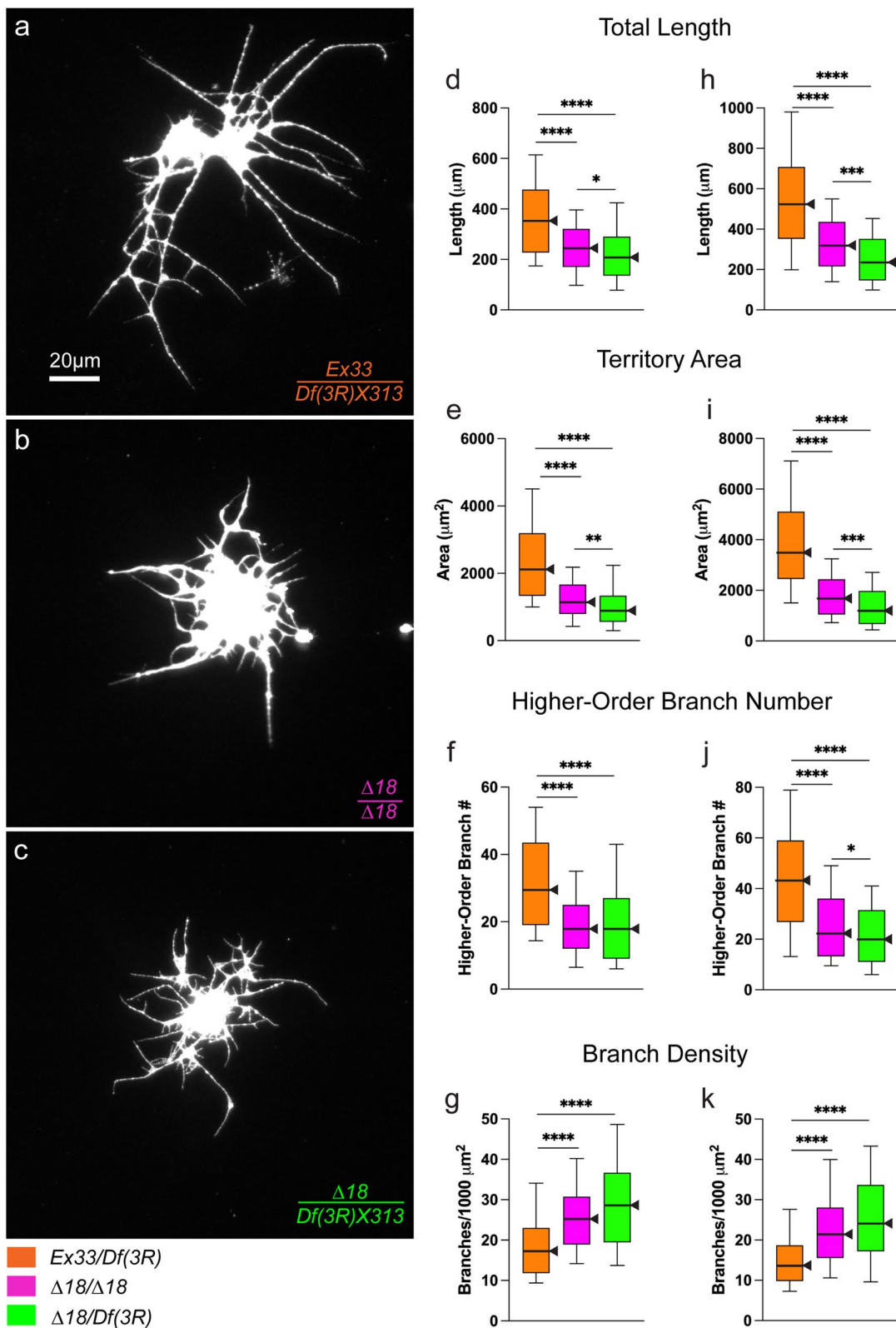


**Fig. 5** (See legend on previous page.)

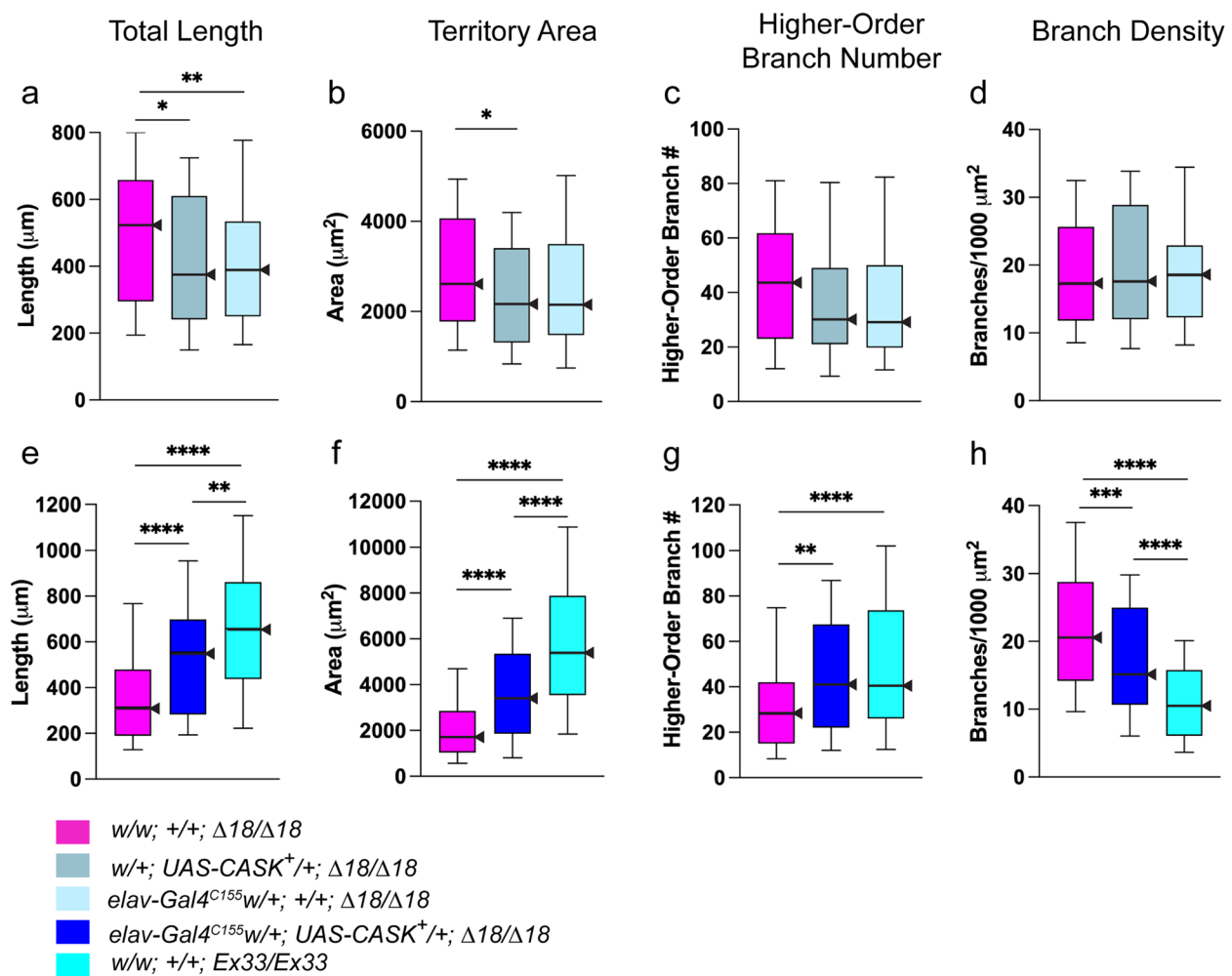


**Fig. 6** Transgenic expression of *CASK<sup>+</sup>* significantly improves the bushy phenotype. Neurite-arbor morphology parameters from 3 div larval CNS neuronal cultures. Box-plot distributions depicted as in Fig. 3. Significance levels: \*,  $p < 0.05$ ; \*\*,  $p < 0.005$ ; \*\*\*,  $p < 0.0005$ ; \*\*\*\*,  $p < 0.00005$ . **a-d** Neither individual transgene, UAS-controlled wild-type full-length *CASK* cDNA or the neuronal driver, *elav-Gal4<sup>C155</sup>*, improved the bushy phenotype of *CASK*-mutant ( $\Delta 18/\Delta 18$ ) neurons. Three genotypes were compared: *w/w; +/+; \Delta 18/\Delta 18* ( $n = 104$ ; magenta); *w/+; UAS-CASK<sup>+/+</sup>; \Delta 18/\Delta 18* ( $n = 104$ ; gray); and *elav-Gal4<sup>C155</sup>w/+; +/+; \Delta 18/\Delta 18* ( $n = 105$ ; light blue). **a** Both transgenes caused modest reductions in total neurite length, i.e., worsening the phenotype. **b** Territory area was mildly reduced by *UAS-CASK<sup>+/+</sup>* only. **c** Higher-order branch number was not affected by either transgene. **d** Branch density, the most distinctive feature of the bushy phenotype, was not affected by either transgene. **e-h** Driving expression of transgenic *CASK<sup>+</sup>* in neurons significantly improved all four parameters of the bushy phenotype. Three genotypes were compared: *w/w; +/+; \Delta 18/\Delta 18* ( $n = 105$ ; magenta); *elav-Gal4<sup>C155</sup>w/+; UAS-CASK<sup>+/+</sup>; \Delta 18/\Delta 18* ( $n = 104$ ; bright blue); and *w/w; +/+; Ex33/Ex33* (*CASK* control;  $n = 105$ ; aqua). **e** Total neurite length. **f** Territory area. **g** Higher-order branch number. **h** Branch density. Strong but incomplete transgenic rescue is consistent with the dosage-sensitive nature of the bushy phenotype

therefore non-fatigable – microfluidics-based method for dissociation of *Drosophila* larval CNS into viable neurons for primary culture [68]. Enzyme-treated tissue was exposed to a controlled oscillating fluid flow that generates a periodic stress field in a microchannel, yielding single-cell suspensions. Here we report on optimization of device design and operation for dissociating *Drosophila* larval CNS tissue. We also demonstrated utility for dissociation of developing rodent CNS.

The microfluidic device conceptual design consists of channels with mirror-image-symmetric layout centered on a narrow constriction zone (“orifice”) (Fig. 7a, b). Transparency of the device allows for real-time monitoring by microscopy. One port is connected to a computer-controlled pump to manipulate the flow field while the other port is used for tissue loading and cell recovery (Fig. 7b, c). Tissue dissociation, driven by bi-directional oscillatory fluid flow,

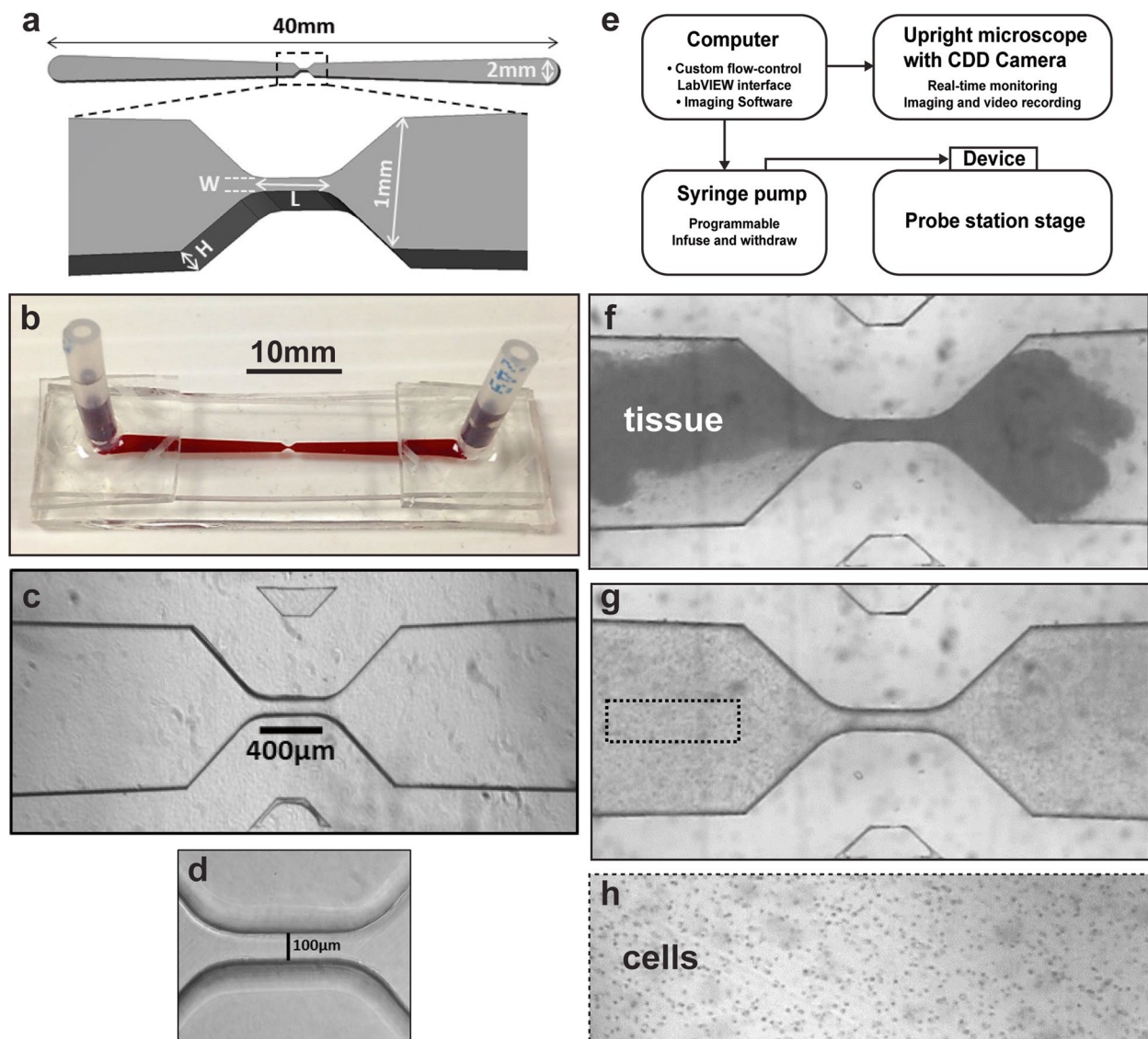


**Fig. 7** A microfluidic system for dissociation of CNS into viable neurons. **a** Schematic drawing of the microdevice, top-down view, with central portion magnified and shown in oblique lateral view. Tissue dissociation takes place in the narrow central orifice. Length (L), width (W), and height (H) were varied during optimization. **b** Photograph of single-channel microfluidic device, lateral oblique view: ports extending upward from the distal ends provide inlet/outlet access and connection to the pump. The channel has been filled with red dye to make it easily visible. **c, d** Photomicrographs of the central part of the channel, top-down views. **c** As the main channel segments approach the central orifice, the walls narrow at 45° angles. **d** High-magnification view of the orifice. Note the smoothness of the channel walls. The 100- $\mu\text{m}$ -wide channels were not needed or used in the experiments reported here. **e** A block diagram illustrating the main components of the experimental system. The microfluidic device sits on the stage of a Signatone probe station equipped with an upright compound microscope and computer-controlled CCD camera. One device port is connected by tubing to a computer-controlled syringe pump that drives oscillatory flow within the channel. **f–h** Individual frames of video acquired during the dissociation of an enzyme-treated piece of rat E18 hippocampus in a microfluidic device. **f** Intact tissue is driven by the pump through the central orifice with dimensions  $L=400\ \mu\text{m}$ ,  $W=70\ \mu\text{m}$ . **g** Following oscillatory cycles of flow-induced shear stress (flow rate  $50\ \mu\text{l}/\text{sec}$ , infusion volume  $12.5\ \mu\text{l}$ , 4 Hz), the tissue has been dissociated into cell clusters and single cells. Dotted rectangle indicates approximate size of the area shown in (h) at a later time at higher magnification. **h** Additional cycles have completed the dissociation into single cells which were collected and plated for culture

occurs in the narrow central orifice (Fig. 7d) within which shear-stress magnitude and gradients are enhanced.

Devices fabricated with varying channel height and central-orifice length and width (Fig. 7a), and operated under varying flow parameters to optimize

dissociation of fruit fly CNS tissue. Once we could achieve apparently full dissociation, by microscopic examination in real time within the device, the outcome measures were (1) completeness of dissociation to single cells, which could be assessed after plating the cells and flooding the dishes, and (2) neuronal health, as evidenced by survival and neurite arbor morphogenesis during culture for several days. For most of the optimization trials, outcome assessments were conducted by daily holistic scoring by an expert in manual dissociation (J.A.T.). Once device and flow parameters were identified that yielded excellent *Drosophila* CNS dissociation, cell recovery, and neurite outgrowth, as assessed by holistic scoring, device trials were performed in parallel with manual dissociation, with the cultured neurons immunostained and imaged for quantitative comparison.

While the orifice length was fixed at 30  $\mu\text{m}$  in previously reported work [68], it was increased to 50, 100, 200, or 400  $\mu\text{m}$  in the current trials, with the longest yielding better and more consistent results. Hence, the large majority of experiments were conducted with an orifice length of 400  $\mu\text{m}$ . Note that the maximum dimension of the *Drosophila* larval CNS is  $\sim 500$   $\mu\text{m}$ . The widths of the central orifice tested were 25, 40, 50, 60, 70, and 80  $\mu\text{m}$ . The channel/orifice heights tested were 350, 400, 450, 490, and 500  $\mu\text{m}$ . The resulting peak shear stress across all trials and tissues ranged from 10 to  $10^4$  dynes/cm<sup>2</sup>. The infusion volumes tested were 10.0, 10.3, 10.4, 10.5 and 12.6  $\mu\text{l}$ , at oscillation frequencies of 3–5 Hz. The flow rates were 50–60  $\mu\text{l/s}$ , occasionally increased to 80  $\mu\text{l/s}$  during the dissociation. The number of cycles varied from  $\sim 300$  to  $\sim 2,000$ , with  $> 15$  points along the range tested.

For *Drosophila* larval CNS, optimal channel height was 450  $\mu\text{m}$ ; optimal orifice dimensions were 400  $\mu\text{m}$  in length and 50  $\mu\text{m}$  in width. Optimal flow parameters were determined to be 10.5  $\mu\text{l}$  for the infusion volume, at 50  $\mu\text{l/sec}$  flow rate, with an oscillation frequency of 5 Hz for 1,400 cycles; total time was  $\sim 5$  min. The resulting dissociations were highly consistent. Within the first 1–2 min, the tissue was reduced to a suspension of cell clusters and individual cells. By the end, the dissociations were complete with few, if any, residual clumps or clusters of cells. Under these optimal conditions, the tissue was transiently exposed to an estimated maximum shear stress of  $\sim 2000$  dynes/cm<sup>2</sup> based on the model presented in Jiang et al. [68]. Compared with our standard manual dissociation protocol [76, 143], the device-based oscillation rate is about five times faster and the cycle number is  $\sim 17$  times higher. These parameters would be impossible to achieve with a manual pipetting device.

Several hours after plating the device-dissociated *Drosophila* larval CNS cells, immunostaining for standard markers revealed that the large majority were neurons, with a small number of glia and some presumed neural stem cells (data not shown). Neuronal health, as evidenced by neurite-arbor morphogenesis during the next several days, was excellent (see next section). As in the case of manually dissociated CNS [143], glia were not present at 3 div. Hence, these are close-to-pure neuronal cultures, with the neurons having a wide range of in vivo developmental histories.

Following optimization of device-based dissociation of fruit fly larval CNS, we tested prenatal (E18) rodent hippocampal tissue. Individual tissue pieces were loaded into each channel (Fig. 7d). Those were at least several fold larger than the maximum dimension of a *Drosophila* larval CNS. Therefore, the channel height was increased to 500  $\mu\text{m}$ , with orifice width increased to 70  $\mu\text{m}$  and orifice length maintained at 400  $\mu\text{m}$ . Similarly, compared to the *Drosophila* protocol, the infusion volume was increased to 12.5  $\mu\text{l}$  (and sometimes as high as 30  $\mu\text{l}$ ), with oscillation frequency somewhat slower at 3–4 Hz for  $\sim 1,000$  cycles. Flow rates of 50–100  $\mu\text{l/sec}$  were effective; dissociation times were 3–6 min. Following dissociation, the estimated cell yield from a pair of E18 rat hippocampi was 1.8 million, which compares favorably with BrainBits<sup>®</sup>/Transnetyx<sup>®</sup> ([https://tissue.transnetyx.com/E18-Rat-Hippocampus\\_4](https://tissue.transnetyx.com/E18-Rat-Hippocampus_4), last accessed 6 December 2022) guarantee of 1 million cells following manual dissociation. After plating, the dissociated hippocampal neurons showed qualitatively good survival and extension of complex arbors (Additional file: Fig. A3). While we did not undertake a full optimization, we did demonstrate that microfluidic dissociation has utility for mammalian CNS.

#### **A microfluidic system for CNS-tissue dissociation reproduces the bushy phenotype of *CASK*-mutant neurons with high fidelity**

When pairs of *Drosophila* neuronal cultures were prepared from CNS of the same genotype, dissociated in parallel in a microdevice versus manually by an expert (J.A.T.), the device-dissociated neurons grew significantly larger neurite arbors (Fig. 8a-f). This was particularly striking for territory area, but total neurite length and higher-order branch number were also increased. The neurite-arbor size difference was evident in neurons of both *CASK* genotypes (control Fig. 8a-c; mutant Fig. 8d-f). These findings suggest that the device-dissociated neurons were healthier, perhaps because they experienced less mechanical trauma. Comparing cultures of neurons dissociated in a single-channel device with those dissociated immediately thereafter in a device consisting of two identical, parallel dissociation channels, we found

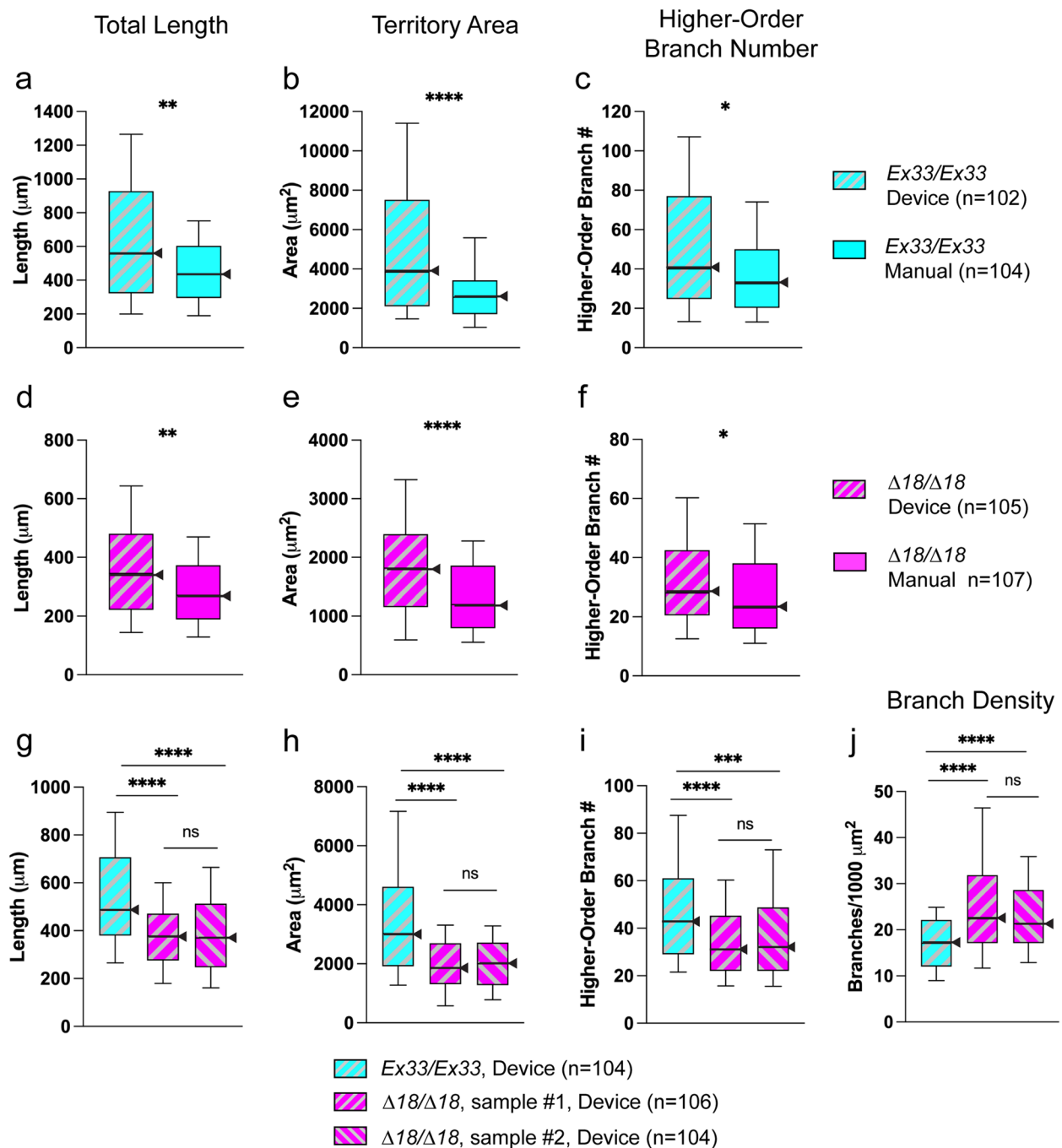


**Fig. 8** Device-dissociated neurons extend larger arbors and manifest the *CASK*-LOF bushy phenotype in vitro. Device dissociations were performed with flow parameters 50  $\mu\text{l}/\text{sec}$ , infusion volume 10.5  $\mu\text{l}$ , 4.8 Hz, mean cycle number 1444. Neurite-arbor size parameters from 3 div cultures, comparing methods of dissociation and genotypes. Box-plot distributions depicted as in Fig. 3. Significance levels: \*,  $p < 0.05$ ; \*\*,  $p < 0.005$ ; \*\*\*,  $p < 0.0005$ ; \*\*\*\*,  $p < 0.00005$ ; ns, not significant. **a-f** Device vs. manual dissociation. **a-c** *Ex33/Ex33*. Device dimensions: channel height 500  $\mu\text{m}$ ; orifice length 400  $\mu\text{m}$ ; orifice width 60  $\mu\text{m}$ . **d-f**  $\Delta 18/\Delta 18$ . Device dimensions: channel height 450  $\mu\text{m}$ ; orifice length 400  $\mu\text{m}$ ; orifice width 50  $\mu\text{m}$ . For both genotypes, total neurite length (**a, d**), territory area (**b, e**), and higher-order branch number (**c-f**) were significantly higher for microfluidic device-dissociated neurons. **g-j** Comparison of device-dissociated neurons from control (*Ex33/Ex33*; one sample) and *CASK* mutant ( $\Delta 18/\Delta 18$ ; two samples) larval CNS. Device dimensions: channel height 450  $\mu\text{m}$ ; orifice length 400  $\mu\text{m}$ ; orifice width 50  $\mu\text{m}$ . **g** Total neurite length. **h** Territory area. **i** Higher-order branches. **j** Branch density. Device-dissociated *CASK*-mutant neurons extend bushy neurite arbors, replicating the phenotype seen in manual cultures. In addition, two cultures prepared after serial device-based dissociation show marked consistency of neurite-arbor parameters

that neurite-arbor parameters did not differ between the two (Additional file: Fig. A4).

In order to make use of the benefits of microdevice-based CNS dissociation, especially for drug screening and studies of *CASK* function, it is essential to determine whether the method modifies the *CASK*-LOF mutant neuronal phenotype. This was of particular concern because of the relatively large arbor size of device-dissociated cultured neurons (Fig. 8a-f). Dissociations were performed in series in single-channel devices using larval CNS tissue from two different *CASK* mutants ( $\Delta I8/\Delta I8$ ) and one control (*Ex33/Ex33*). Compared with control neurons, the *CASK*-mutant neurons extended smaller, denser neurite arbors, with high levels of statistical significance for all parameters (Fig. 8g-j). This replicates the *CASK*-mutant bushy phenotype. In *CASK*-mutant cultures from the two sequential dissociations shown, device-dissociated  $\Delta I8/\Delta I8$  neurons had markedly similar neurite arbors with no statistically significant differences in any parameter. Hence, device dissociation yields excellent consistency and does not alter the *CASK* phenotype.

## Discussion

### The challenge of reconciling *CASK* biochemistry, cell biology, and human genetics

*CASK* defies simple classification. It is a highly conserved member of the MAGUK (Membrane-Associated Guanylate Kinase) protein family [31, 82], this study), based on the presence and order of its three C' domains: PDZ, SH3 (Src homology 3) and GUK (guanylate kinase). Like other MAGUKs [44], *CASK* acts as a scaffold that tethers and localizes adhesion molecules, receptors, and signaling molecules [59, 106]. However, the name *CASK*, an acronym for calcium/calmodulin-dependent serine protein kinase, is based on sequence similarity of its N'-terminal domain, which is unique among MAGUK family members [53]. Given that *CASK* does not have typical CaMK activity, this name is problematic. *CASK* was classified as a pseudokinase because its CaMK-like N' domain lacks a DFG motif (Asp-Phe-Gly) which is required for Mg<sup>2+</sup>-binding and was thought to be essential for kinase activity [12]. However, *CASK*'s CaMK-like N' domain can catalyze Mg<sup>2+</sup>-independent phosphorylation [109] of neuexin-1, a *CASK* binding partner [53]. Thus, *CASK* has at least two distinct molecular functions, scaffolding and enzymatic, both involving presynaptic neuexin. The third is transcriptional regulation, via partnership with co-activators [59].

The human phenotypes of *CASK*-related disorders have a remarkable range of clinical severity and manifestations, none of which has been conclusively ascribed to specific molecular functions. The most consistent phenotypes are

intellectual disability (ID) and microcephaly with hind-brain predominance. Microcephaly is common in monogenic ID disorders (occurring in ~40% based on OMIM Clinical Synopsis pages; data not shown), as is variable expressivity and incomplete penetrance. Indeed, most of the disorders caused by mutations in *CASK* partner genes have microcephaly as a feature (Additional file: Table A1). Among children with *CASK*-related disorders, progressive postnatal microcephaly has been extensively documented. In addition, congenital microcephaly has been reported in a substantial minority of cases (e.g., [15, 104, 112, 134, 149]). Hence, *CASK* function in the human CNS starts prenatally, aligning with highest *CASK* transcript accumulation in the prenatal brain and a gradual decline in all brain regions over the lifespan (Human Brain Transcriptome project, <https://hbatlas.org/hbtd/images/wholeBrain/CASK.pdf>, last accessed 3 January 2023; [69]). *CASK* is expressed in many other organs as well (NCBI; <https://www.ncbi.nlm.nih.gov/gene/8573>, last accessed 10 January 2023). Common phenotypes outside the CNS may include short stature and mild facial dysmorphism [103, 104, 149].

Much of the molecular and cellular analysis of *CASK* function has focused on neurons at advanced stages of differentiation to study synapse formation and physiology, sometimes alongside investigations of partner proteins [59]. This focus reflects the history of *CASK*'s discovery, its localization to both sides of the mature synapse, and its binding to numerous synaptic proteins. For example, based on acute RNA interference, cultured hippocampal neurons required *CASK* for normal size and density of dendritic spines [19]. Cultured cortical neurons from transgenic *CASK*-KO newborn mice showed abnormal rates of spontaneous synaptic release events, elevated for excitatory (glutamatergic) and reduced for inhibitory (GABAergic), but with no change in evoked release or synapse ultrastructure [8]. Similarly, in acutely cultured brain slices from heterozygous *CASK*-KO mice (functionally mosaic, like human females with MICPCH), miniature excitatory/inhibitory (E/I) postsynaptic currents were increased/decreased, respectively, but only in the *CASK*-deficient neurons [105]. Retinogeniculate synapses of *CASK*-heterozygous mice showed reductions in active zone numbers [88]. Synaptic physiology abnormalities were also demonstrated in *CASK*-LOF *Drosophila* [21, 48, 147, 168]. When human embryonic stem cells (hESC) were used to create a *CASK*-null condition by gene editing, the mutant cortical excitatory neurons differentiated from them showed defective synaptic transmission and network activity [99]. Evidence of E/I imbalance in humans with *CASK*-related disorders came from synapses of neurons differentiated from *CASK*-mutant induced pluripotent stem cells (iPSc), showing

reduced size of inhibitory presynaptic sites, as well as from in vivo brain imaging by magnetic resonance spectroscopy showing low levels of GABA [10].

On the other hand, synaptic dysfunction cannot explain reduced brain size especially when it starts in utero. The brainstem and cerebellum are exquisitely sensitive to *CASK*-LOF, with markedly reduced volume detectable in early postnatal MRIs of children with MICPCH. The brainstem defects are believed to cause hypoventilation, potentially fatal [8]. Two neonatal autopsies revealed minimal formation of cerebellar folia, marked loss of cerebellar granule cells, and astrogliosis consistent with prior neurodegeneration [112, 120]. The hypoplasia of severe MICPCH extends beyond hindbrain structures. Published MRIs show cortical volume reduction, simplification of gyral patterns, and corpus callosum abnormalities (e.g., [57, 103, 108, 112, 113, 118, 128, 148]). The variable phenotypes of optic nerve hypoplasia and retinopathy [71, 80, 112] also reflect disrupted early forebrain development. By histopathology of a two-week-old male, the cerebral cortex showed lamination defects selectively affecting layers V and VI [112]. These layers express TBR1, a transcriptional co-activator which partners with *CASK* to up-regulate *RELN* expression [60]. These phenotypes are not causally related to proposed synaptic functions of *CASK*. Indeed, analysis of several types of transgenic *CASK*-mutant mice implicate non-neuronal cells as contributors to microcephaly [145].

As for neuronal microanatomy, there are no reported Golgi-impregnation studies in any species with *CASK* LOF. McSweeney et al. [99] evaluated neurite arbors of *CASK-KO* neurons differentiated from gene-edited hESC. Early during differentiation, neurons showed increased dendritic branch points; dendritic length was not consistently altered and branch density was not reported. In co-cultures with murine wild-type glia, mature neurons had normal-sized dendritic arbors. Increased branch complexity of differentiating *CASK-KO* human neurons in vitro aligns with the bushy phenotype.

The CNS phenotypes of *CASK*-related disorders are likely to result from both cell-autonomous and non-cell-autonomous primary defects, with a cascade of secondary effects on brain development, worsened by functional disruptions of neural circuitry [107]. For example, *CASK*-LOF altered transcript profiles in mouse brain [121], in neurons differentiated from patient-specific iPSc lines or siRNA-mediated knockdown in controls [10] or differentiated from gene-edited hESC [99]. In *CASK*-heterozygous mouse brain, where X inactivation leads to interactions between wild-type and mutant cells, marked changes in the proteome, affecting many pathways, suggest a stepwise expansion of the effects of *CASK*-LOF [121]. Non-cell-autonomous effects could arise by

cell–cell interactions, e.g., trans-synaptic or neuron–glia. Impaired metabolism has also been reported in *CASK*-heterozygous mice [145]. In contrast, *Drosophila CASK* mutants have normal oxygen consumption on a per-mg basis [42].

#### Multi-level alignment of human and fruit fly *CASK*: genetics and neurobiology

The value of the *Drosophila* genetic model system for studying neurodevelopmental disorders is well-recognized [7, 22, 90, 97]. Work from multiple groups has documented cognitive and motor-behavior phenotypes in *Drosophila* with *CASK*-LOF or absence [6, 48, 95, 96, 142]. When the design of those studies allowed, behavioral phenotypes were sensitive to *CASK* dosage, as in humans. Memory or learning defects in *CASK*-LOF larvae or flies using appetitive or aversive associative learning paradigms [48, 95] provide face validity for the ID of *CASK*-related disorders. Stereotyped repetitive grooming behavior may be relevant to a core symptom of ASD [6], which can be seen with human *CASK*-LOF [10, 64, 139].

At the biochemical level, *Drosophila CASK* promotes autophosphorylation of CaMKII. In *Caki* mutant flies (with overlapping deletions), human *CASK*<sup>+</sup> can rescue the CaMKII-autophosphorylation defect [48]. Like mammalian *CASK*, the fruit fly ortholog has many binding partners, a majority are specific to neuronal subsets [110]. X inactivation is not an issue, because *Drosophila CASK* is not X-linked and the mechanism of dosage compensation is different. The lack of mosaicism in *CASK* heterozygous *Drosophila*, cf., in human females, could be of benefit.

We have discovered a small-brain phenotype in *Drosophila* with *CASK*-LOF. This is evident by eye midway through development (Fig. 3a) and persists through late metamorphosis (Fig. 2e). Thus, the requirement of *CASK*<sup>+</sup> for normal brain-size acquisition is highly conserved among humans [102], mice [145], zebrafish [24], and now fruit flies. We found no obvious indication of reduced neuronal numbers in *CASK*-mutant larval CNS. Blinded full-dish counts of cultured neurons of three genotypes showed only modest differences (within 4–5%) among  $\Delta 18/\Delta 18$  mutant, *Ex33/Ex33* controls, and  $\Delta 18/\Delta 18$  with one copy of *CASK*<sup>+</sup> (data not shown). With the caveat that neurogenesis and programmed cell death have not been assessed, these preliminary data suggested that diminished neuron numbers do not explain the gross reduction in *CASK*-mutant CNS size.

We also demonstrated that acquisition of normal *Drosophila* body length requires *CASK*<sup>+</sup> function (Fig. 2c). This is consistent with a statistically significant reduction in body weight of  $\Delta 18/\Delta 18$  compared with *Ex33/Ex33* [42]. The similarity of puparium length and mammalian

CRL as measures of axial growth has several dimensions. In humans, first-trimester CRL reflects gestational age [123]. Conversely, reduced CRL may be associated with developmental abnormalities of genetic or environmental origin [11, 54, 138, 164]. A set of phylogenetically conserved transcription factors, originally discovered in *D. melanogaster*, control growth and development along the longitudinal axis of insects and vertebrates [18, 50]. Thus, while not precisely analogous to stature, puparium length nonetheless provides an excellent measure of fruit fly body length at a midway point during development. The combination of microcephaly, a form of 'short stature', and impaired cognition represents strong face validity of the *Drosophila* model of *CASK*-related disorders. To understand the cellular basis of microencephaly in *CASK*-LOF *Drosophila*, we turned to primary neuronal cell culture.

#### The bushy phenotype of *CASK*-mutant neurite arbors

"Bushy" is a specific small-arbor phenotype in which primary size parameters are reduced but with increased branch density (e.g., Fig. 3i-l), including both branches per unit area and branches per unit length (Additional file: Table A2). Qualitatively, the bushy phenotype is reminiscent of the *tumbleweed*-mutant dendritic arbors of sensory neurons [46]. Three other small-arbor mutant phenotypes of that we have characterized in vitro have markedly different features. *Pak* LOF causes small, sparse arbors [87], while *CBP/nejire* LOF causes a very severe 'naked-arbor' defect (K. Olsen, R. Kraft, and L.L.R., unpublished). Finally, *fascin/singed* LOF causes the "filagree" phenotype, with marked curvature of neurites and a small territory despite normal length [74, 75].

Because primary neurite numbers were unchanged by *Drosophila CASK* LOF, while higher-order branches and total neurite length were markedly reduced, we infer that neurite initiation from the neuronal cell body was normal, but neurite elongation was deficient. We further infer that branch formation, either interstitial or at growth cones, occurred prematurely, leading to increased branch density. Because our cell culture system is low density and nearly-all-neuronal, bushy neurite arbors must reflect intrinsic properties of mutant neurons. However, they may not be strictly speaking cell-autonomous because prior to dissociation, the neurons had spent considerable developmental time in contact with each other and with glia. Hence, the bushy phenotype may derive in part from cell-cell interactions earlier in life.

We hypothesize that the in vitro bushy phenotype reflects small dendritic and axonal arbors in vivo which, in turn, contribute to microencephaly in *CASK*-LOF

*Drosophila*. In preliminary studies staining for the pre-synaptic marker Bruchpilot, we noted that larval CNS of  $\Delta 18$  homozygotes appeared to have reduced synaptic neuropil volume relative to brain-lobe volume (data not shown). It may also be that the impact of modestly reduced neuronal number is amplified by reduced arborization within neuropils.

To our knowledge we are the first to report on neurite-arbor morphogenesis in primary neuronal cultures prepared from animals with germline *CASK*-LOF mutations. The bushy phenotype has two mammalian correlates. First, in a *CASK*-overexpression context, transfection with wild-type *CASK* promoted neurite outgrowth by cultured neurons differentiated from mouse Neuro2A cells [157]. Second, short-term culture of neurons differentiated from gene-edited *CASK*-KO hESC showed increased neurite branching [99]. Using a different protocol that included wild-type mouse glia, longer-term neuronal cultures had normal branching (*op. cit.*), perhaps due to rescue by glia.

Elaboration and pruning of cortical neuron dendritic arbors are phases of brain development that, of necessity, impact the architecture of neural circuits. These differentiation processes are disrupted in many ID disorders, resulting in abnormalities of dendritic arbor size and shape [30, 70, 78, 125]. In conjunction with abnormal axonal projections, notably those involving the corpus callosum [35], faulty dendritic arbors plausibly contribute to functionally altered neural circuits and underlie deficits in cognitive development [125]. In *Drosophila Pak*-mutant neurons, the sparse neurite arbors seen in vitro [87] align with the reduced cortical neuron dendritic arbors of mouse *Pak* mutants in vivo, likely via actin cytoskeleton dysregulation [63]. Males with *PAK3* mutations have ID with microcephaly (MIM #300558; <https://omim.org/entry/300558>, last accessed 20 August 2023). We predict that the *Drosophila CASK*-LOF bushy phenotype will align with in vivo neuronal abnormalities of the human *CASK*-LOF CNS.

The specificity of the bushy neurite-arbor defect make cultured *CASK*-LOF neurons an attractive cell-based assay to study pathogenic mechanisms and to screen for modifying compounds of therapeutic value. Starting with an insect model supports the 'Three Rs' goal of reducing use of vertebrate research animals [116]. Given the many potential molecular functions of *CASK*, a cell-based assay would have major advantages over standard medicinal chemistry strategies. First, an unbiased phenotypic screen does not require knowing which protein(s) or signaling pathways should be targeted to improve brain development and function in children with *CASK*-related disorders. Second, recently synthesized *CASK* inhibitors

[133] may have benefit in treating gastrointestinal cancers [33, 126, 158, 167] but would not help *CASK*-LOF neurodevelopmental disorders. In order to efficiently identify enhancers of *CASK*-dependent neurite-arbor morphogenesis, we developed a new method for preparation of primary neuronal cultures.

#### **A technological breakthrough: overcoming the roadblock of CNS tissue dissociation**

We have developed a microfluidic system for automated, standardized, non-fatigable dissociation of brain tissue that yields healthy viable neurons for in vitro cell culture. The arbors elaborated after microfluidic dissociation have excellent quantitative consistency and recapitulate the *CASK*-mutant bushy phenotype (Fig. 8g-j). Moreover, arbors of all genotypes are larger, suggesting the neurons are healthier (Fig. 8a-f). This significant, novel advance follows more than fifty years during which brain-neuron dissociation for primary culture has been an art form, a skill learned at the bench with expert tutelage and much practice. The earliest attempts at separation of individual viable neurons was by extrusion of explanted tissue through a nylon mesh, supplemented by protease treatment and repeated aspiration in media through a Pasteur pipet tip [98, 155, 165]. Decades later, the method still relies on manual trituration of enzyme-treated brain tissue, sometimes using volume-adjustable laboratory pipets, and with the residual-cell-cluster problem being hidden by filtration-based removal [26, 27].

The persistent use of manual dissociation of neural tissues is a testament to the power of primary neuronal culture to advance the understanding of differentiation, synaptic physiology, neurotoxicology, neuropharmacology, and disease pathogenesis [17, 20, 38, 84, 101, 117, 122, 154]. Moreover, several proof-of-concept studies have demonstrated the utility of primary cultured neurons for drug discovery [2, 75, 156, 159]. A compound we identified as an enhancer of the filagreed defect of fascin-deficient neurons [75] was validated independently as a fascin-1 inhibitor [4]. Thus, the potential value of our microfluidic system is high for basic and applied neuroscience, and answers an editorial call for more collaboration between geneticists and engineers [1].

Manual neural tissue dissociation has been a 'black box.' The tissue quickly becomes invisible and there is no way to control the applied force, which has to overcome the extracellular matrix and the connections among neurons. Too much trituration reduces neuronal viability, too little leaves cell clusters intact. Even worse, trituration is fatiguing to the dominant hand which limits the number of samples that can be prepared. For CNS tissue from both *Drosophila* and

rodents, a controlled bi-directional oscillating flow field through a narrow orifice allows tissue dissociation into viable neurons using cycle frequencies and numbers that would be impossible to generate manually. Moreover, the process can be directly observed in real time (Fig. 7d). The most impactful design improvement was an order of magnitude increase in the length of the orifice in which the dissociation takes place, resulting in a longer time interval during which flow shear stress was exerted on the tissue. The microfluidic system could also dissociate neonatal rat (P1) heart tissue, which tolerated higher stress loads (data not shown).

#### **Toward high-throughput drug screening using primary neuronal cultures**

Due to the increasing availability of massively parallel DNA sequencing in the clinic [161], *CASK*-related and other rare disorders are becoming ever-easier to diagnose [73]. While early molecular diagnosis is of high value, especially when paired with genetic counseling [39], prompt initiation of therapy to enhance brain and cognitive development is an important goal. As with Duchenne/Becker muscular dystrophy [25], one initial strategy would be to convert a severe *CASK* phenotype to a mild one. Together, our discoveries of the *CASK*-LOF bushy neurite-arbor phenotype and an automated microfluidic system for CNS tissue dissociation provide a novel cell-based assay for first-line drug discovery. There are precedents for applying microsystems technology to cell-based assays for drug screening [28, 166] to identify small molecules [152], peptides [114, 163], or antibodies [45, 140]. Compounds that improve the bushy phenotype of mutant *Drosophila* neurons in vitro would then be candidates for testing in other *CASK*-LOF animal models or human neurons from iPSc lines.

*CASK* disorders represent a prime target for drug discovery, not only because of the obvious unmet medical need but also because of *CASK* is the hub of a genetic regulatory network. These dozen proteins have essential functions in brain and cognitive development, including acquisition of normal brain size (Additional file: Table A1). Drugs that boost *CASK* function may also be beneficial for disorders caused by mutations in *CASK*-partner genes.

#### **Abbreviations**

ASD	Autism spectrum disorder
βgal	β-Galactosidase
CNS	Central nervous system
CRL	Crown-rump length
div	Days in vitro
E/I	Excitatory/inhibitory
FBS	Fetal bovine serum

hESC	Human embryonic stem cells
ID	Intellectual disability
iPSc	Induced pluripotent stem cell(s)
KO	Knockout
LOF	Loss of function
MAGUK	Membrane-associated guanylate kinase
MICPCH	Microcephaly with pontine-cerebellar hypoplasia
PDMS	Polydimethylsiloxane
w3L	Wandering third instar larva(e)

## Supplementary Information

The online version contains supplementary material available at <https://doi.org/10.1186/s13064-023-00174-y>.

**Additional file 1: Table A1.** CASK Binding Partners and Target Genes linked to Neurodevelopmental Disease.

**Additional file 2: Table A2.** Case reports and series of CASK-related disorders.

**Additional file 3: Table A3.** Effects of CASK LOF mutation on neurite-arbor morphology: analysis across nine experiments.

**Additional file 4: Figure A1.** Amino acid sequence comparison of human and fruit fly CASK.

**Additional file 5: Figure A2.** Frequency distributions of neurite-arbor parameters of CASK-mutant vs. -control neurons.

**Additional file 6: Figure A3.** Rat E18 hippocampal neurons cultured after dissociation in microfluidic devices.

**Additional file 7: Figure A4.** Consistency of neurite-arbor parameters of neurons dissociated in single- vs. twinchannel microfluidic devices.

## Acknowledgements

The authors thank neuroscience students Monica Chaung, Hannah Schmitz, Cecilia Brown, Lauren Pisani, and Rachel Bear for assistance with lab experiments; Moriah Gottman for analysis of ID and microcephaly in OMIM; engineering students Kenneth Decker and Pengcheng Cai for conducting many microdevice trials; Dr. Wulfila Gronenberg for help with adult head histology; Dr. Dean Billheimer, Kyle Humphrey, and Nathan Grunow for guidance on use of linear mixed effects modeling for statistical analyses; Dr. Daniel Gray for advice on 3D data display; Drs. Robert Kraft, David R. Andrew, A. John Clark, Jane PEPARD, Gerald M. Maggiora, Sara A. Lewis, and Kathleen K. Siwicki for helpful discussions on experiments and data; Anna Burns and Dr. Lynne Oland for advice on neuronal cell culture; and Dr. Jennifer K. Inlow for guidance on sequence comparisons.

## Authors' contributions

All four authors contributed to research design and data analysis, with emphasis on neurobiological experiments (J.A.T., L.L.R.) or microfluidic technology development (J.L., Y.Z.). J.A.T. and L.J. conducted experiments. J.A.T. wrote software. J.A.T., L.L.R., and L.J. designed figures and tables. All four authors participated in drafting, editing, and reviewing the manuscript.

## Funding

Funding support for this work was provided by TechLaunch Arizona (J.L., L.L.R., and Y.Z.), a Fulbright Foreign Student Program scholarship (J.A.T.), and the Jérôme Lejeune Foundation (Research grant #1555 to L.L.R.)

## Availability of data and materials

*Drosophila* stocks used in these studies are available from the corresponding author and/or the Bloomington *Drosophila* Stock Center. The data generated and analyzed for this research will be made available by the authors upon reasonable request.

## Declarations

### Ethics approval and consent to participate

Not applicable.

### Consent for publication

Not applicable.

### Competing interests

The authors declare no competing interests.

### Author details

<sup>1</sup>Graduate Interdisciplinary Program in Neuroscience, University of Arizona, Tucson, AZ 85721, USA. <sup>2</sup>Department of Neurology, University of Arizona Health Sciences, 1501 N. Campbell Ave, Tucson, AZ 85724-5023, USA. <sup>3</sup>Present address: Department of Molecular Pathobiology, College of Dentistry, New York University, New York, NY 10010, USA. <sup>4</sup>Department of Aerospace and Mechanical Engineering, University of Arizona, Tucson, AZ 85721, USA. <sup>5</sup>Department of Biomedical Engineering, University of Arizona, Tucson, AZ 85721, USA. <sup>6</sup>BIO5 Interdisciplinary Research Institute, University of Arizona, Tucson, AZ 85721, USA. <sup>7</sup>Department of Cellular & Molecular Medicine, University of Arizona Health Sciences, Tucson, AZ 85724, USA.

Received: 20 August 2023 Accepted: 8 September 2023

Published online: 07 October 2023

## References

- Anonymous, editors. Geneticist seeks engineer: must like flies and worms. *Nat Methods*. 2007;4(6):463. <https://www.nature.com/articles/nmeth0607-463>.
- Al-Ali H, Blackmore M, Bixby JL, Lemmon VP. High content screening with primary neurons. 2013 [updated 2014 Oct 1]. In: Markossian S, Grossman A, Brimacombe K, et al, editors. *Assay Guidance Manual* [Internet]. Bethesda (MD): Eli Lilly & Company and the National Center for Advancing Translational Sciences. NCBI Bookshelf ID: NBK169433. <https://www.ncbi.nlm.nih.gov/books/NBK169433/>. Accessed 20 Aug 2023.
- Al-Mofty S, Elsayed M, Ali H, Ahmed O, Altayyeb A, Wahby A, et al. A microfluidic platform for dissociating clinical scale tissue samples into single cells. *Biomed Microdevices*. 2021;23:10.
- Albuquerque-González B, Bernabé-García M, Montoro-García S, Bernabé-García Á, Rodrigues PC, Ruiz Sanz J, et al. New role of the anti-depressant imipramine as a Fascin1 inhibitor in colorectal cancer cells. *Exp Mol Med*. 2020;52:281–92.
- Aliaghaei M, Haun JB. Optimization of mechanical tissue dissociation using an integrated microfluidic device for improved generation of single cells following digestion. *Front Bioeng Biotechnol*. 2022;10: 841046.
- Andrew DR, Moe ME, Chen D, Tello JA, Doser RL, Conner WE, et al. Spontaneous motor-behavior abnormalities in two *Drosophila* models of neurodevelopmental disorders. *J Neurogenet*. 2021;35:1–22.
- Androschuk A, Al-Jabri B, Bolduc FV. From learning to memory: What flies can tell us about intellectual disability treatment. *Front Psychiatry*. 2015;6:85.
- Atasoy D, Schoch S, Ho A, Nadasy KA, Liu X, Zhang W, et al. Deletion of CASK in mice is lethal and impairs synaptic function. *Proc Natl Acad Sci U S A*. 2007;104(7):2525–30.
- Bainbridge SP, Bownes M. Staging the metamorphosis of *Drosophila melanogaster*. *J Embryol Exp Morphol*. 1981;66:57–80.
- Becker M, Mastropasqua F, Reising JP, Maier S, Ho ML, Rabkina I, et al. Presynaptic dysfunction in CASK-related neurodevelopmental disorders. *Transl Psychiatry*. 2020;10:312.
- Bora SA, Bourne T, Bottomley C, Kirk E, Papageorghiou AT. Twin growth discrepancy in early pregnancy. *Ultrasound Obstet Gynecol*. 2009;34:38–42.
- Boudeau J, Miranda-Saavedra D, Barton GJ, Alessi DR. Emerging roles of pseudokinases. *Trends Cell Biol*. 2006;16:443–52.
- Brand AH, Dormand EL. The GAL4 system as a tool for unravelling the mysteries of the *Drosophila* nervous system. *Curr Opin Neurobiol*. 1995;5:572–8.
- Brown C. Genetic requirements for building a brain of a sufficient size: insights from Mendelian congenital microcephaly disorders. Tucson: Masters thesis, University of Arizona; 2017.
- Burglen L, Chantot-Bastarud S, Garel C, Milh M, Touraine R, Zanni G, et al. Spectrum of pontocerebellar hypoplasia in 13 girls and boys with

- CASK mutations: confirmation of a recognizable phenotype and first description of a male mosaic patient. *Orphanet J Rare Dis.* 2012;7:18.
16. Butz S, Okamoto M, Südhof TC. A tripartite protein complex with the potential to couple synaptic vesicle exocytosis to cell adhesion in brain. *Cell.* 1998;94:773–82.
  17. Cao Z, Shafer TJ, Crofton KM, Gennings C, Murray TF. Additivity of pyrethroid actions on sodium influx in cerebrocortical neurons in primary culture. *Environ Health Perspect.* 2011;119:1239–46.
  18. Cecchi C, Mallamaci A, Boncinelli E. Otx and Emx homeobox genes in brain development. *Int J Dev Biol.* 2000;44:663–8.
  19. Chao HW, Hong CJ, Huang TN, Lin YL, Hsueh YP. SUMOylation of the MAGUK protein CASK regulates dendritic spinogenesis. *J Cell Biol.* 2008;182:141–55.
  20. Chen J, Herrup K. Selective vulnerability of neurons in primary cultures and in neurodegenerative diseases. *Rev Neurosci.* 2008;19:317–26.
  21. Chen K, Featherstone DE. Pre and postsynaptic roles for *Drosophila* CASK. *Mol Cell Neurosci.* 2011;48(2):171–82.
  22. Coll-Tané M, Krebbers A, Castells-Nobau A, Zweier C, Schenck A. Intellectual disability and autism spectrum disorders 'on the fly': insights from *Drosophila*. *Dis Model Mech.* 2019;12:dmm039180.
  23. Conway K, Kiernan JA. Chemical dehydration of specimens with 2,2-dimethoxypropane (DMP) for paraffin processing of animal tissues: practical and economic advantages over dehydration in ethanol. *Biotech Histochem.* 1999;74:20–6.
  24. Cristofoli F, Devriendt K, Davis EE, Van Esch H, Vermeesch JR. Novel CASK mutations in cases with syndromic microcephaly. *Hum Mutat.* 2018;39:993–1001.
  25. Crudele JM, Chamberlain JS. AAV-based gene therapies for the muscular dystrophies. *Hum Mol Genet.* 2019;28(R1):R102–7.
  26. Darbinyan A, Kaminski R, White MK, Pozniak PD, Darbinian N, Khalili K. Isolation and propagation of primary human and rodent embryonic neural progenitor cells and cortical neurons. *Methods Mol Biol.* 2021;2311:51–61.
  27. de Prisco N, Chemiakine A, Lee W, Botta S, Gennarino VA. Protocol to assess the effect of disease-driving variants on mouse brain morphology and primary hippocampal neurons. *STAR Protoc.* 2022;3:101244.
  28. De Stefano P, Bianchi E, Dubini G. The impact of microfluidics in high-throughput drug-screening applications. *Biomicrofluidics.* 2022;16:031501.
  29. Deciphering Developmental Disorders Study. Prevalence and architecture of de novo mutations in developmental disorders. *Nature.* 2017;542:433–8.
  30. Dierssen M, Ramakers GJ. Dendritic pathology in mental retardation: from molecular genetics to neurobiology. *Genes Brain Behav.* 2006;5(Suppl 2):48–60.
  31. Dimitratos SD, Woods DF, Bryant PJ. Camguk, Lin-2, and CASK: novel membrane-associated guanylate kinase homologs that also contain CaM kinase domains. *Mech Dev.* 1997;63(1):127–30.
  32. Dimitratos S. Cloning and characterization of *camguk* (*cmg*), a member of the Membrane-Associated Guanylate Kinase (MAGUK) protein family, and mapping of the human *cmg* ortholog, *CASK*. Doctoral dissertation, University of California - Irvine; 1999.
  33. Ding B, Bao C, Jin L, Xu L, Fan W, Lou W. CASK silence overcomes sorafenib resistance of hepatocellular carcinoma through activating apoptosis and autophagic cell death. *Front Oncol.* 2021;11: 681683.
  34. Dunn P, Prigatano GP, Szelingier S, Roth J, Siniard AL, Claasen AM, et al. A de novo splice site mutation in CASK causes FG syndrome-4 and congenital nystagmus. *Am J Med Genet A.* 2017;173:611–7.
  35. Edwards TJ, Sherr EH, Barkovich AJ, Richards LJ. Clinical, genetic and imaging findings identify new causes for corpus callosum development syndromes. *Brain.* 2014;137(Pt 6):1579–613.
  36. Edwards CA, Walker GK, Booth HD, Fredenburgh J. The use of 2,2 dimethoxypropane in rapid dehydration of tissues for light microscopy. *J Histotechnology.* 1979;2(3):114–6.
  37. Elgin S, Miller D. Mass rearing of flies and mass production and harvesting of embryos. *The Genetics and Biology of Drosophila.* Vol. 2a. New York: Academic Press; 1978. p. 112–21.
  38. Ellen CW, Mercer AR. Modulatory actions of dopamine and serotonin on insect antennal lobe neurons: insights from studies in vitro. *J Mol Histol.* 2012;43(4):401–4.
  39. Elliott AM. Genetic counseling and genome sequencing in pediatric rare disease. *Cold Spring Harb Perspect Med.* 2020;10(3):a036632.
  40. Fay MP, Proschan MA. Wilcoxon-Mann-Whitney or t-test? On assumptions for hypothesis tests and multiple interpretations of decision rules. *Stat Surv.* 2010;4:1–39.
  41. Fletcher JC, Thummel CS. The *Drosophila* E74 gene is required for the proper stage- and tissue-specific transcription of ecdysone-regulated genes at the onset of metamorphosis. *Development.* 1995;121:1411–21.
  42. Ford SR, Flores JI, Sandstrom DJ. Measuring O2 consumption in *Drosophila melanogaster* using coulometric microrespirometry. *J Vis Exp.* 2023;(197). <https://doi.org/10.3791/65379>.
  43. Fristrom D, Fristrom J. The metamorphic development of the adult epidermis. In: Bate M, Martinez Arias A, editors. *The Development of Drosophila melanogaster.* Cold Spring Harbor Laboratory: Cold Spring Harbor, NY; 1993. p. 843–97.
  44. Funke L, Dakoqi S, Brecht DS. Membrane-associated guanylate kinases regulate adhesion and plasticity at cell junctions. *Annu Rev Biochem.* 2005;74:219–45.
  45. Gaa R, Menang-Ndi E, Pratapa S, Nguyen C, Kumar S, Doerner A. Versatile and rapid microfluidics-assisted antibody discovery. *MAbs.* 2021;13(1):1978130.
  46. Gao FB, Brenman JE, Jan LY, Jan YN. Genes regulating dendritic outgrowth, branching, and routing in *Drosophila*. *Genes Dev.* 1999;13:2549–61.
  47. Giacomini T, Nuovo S, Zanni G, Mancardi MM, Cusmai R, Pepi C, et al. CASK related disorder: Epilepsy and developmental outcome. *Eur J Paediatr Neurol.* 2021;31:61–9.
  48. Gillespie JM, Hodge JJ. CASK regulates CaMKII autophosphorylation in neuronal growth, calcium signaling, and learning. *Front Mol Neurosci.* 2013;6:27.
  49. González-Roca I, Alonso-Rivero P, Sánchez-Sobechero A, Vázquez-López M. New mutation in the CASK gene in a child with microcephaly syndrome and pontocerebellar hypoplasia. *Rev Neurol.* 2020;71(4):161–2.
  50. Gruss P, Kessel M. Axial specification in higher vertebrates. *Curr Opin Genet Dev.* 1991;1:204–10.
  51. Gupta P, Shinde A, Illath K, Kar S, Nagai M, Tseng FG, et al. Microfluidic platforms for single neuron analysis. *Mater Today Bio.* 2022;13: 100222.
  52. Hackett A, Tarpey PS, Licata A, Cox J, Whibley A, Boyle J, et al. CASK mutations are frequent in males and cause X-linked nystagmus and variable XLMR phenotypes. *Eur J Hum Genet.* 2010;18:544–52.
  53. Hata Y, Butz S, Südhof TC. CASK: a novel dlg/PSD95 homolog with an N-terminal calmodulin-dependent protein kinase domain identified by interaction with neuroligins. *J Neurosci.* 1996;16(8):2488–94.
  54. Hayama SI, Tsuchiya M, Ochiai K, Nakiri S, Nakanishi S, Ishii N, Kato T, Tanaka A, Konno F, Kawamoto Y, Omi T. Small head size and delayed body weight growth in wild Japanese monkey fetuses after the Fukushima Daiichi nuclear disaster. *Sci Rep.* 2017;7:3528.
  55. Hayashi S, Mizuno S, Migita O, Okuyama T, Makita Y, Hata A, et al. The CASK gene harbored in a deletion detected by array-CGH as a potential candidate for a gene causative of X-linked dominant mental retardation. *Am J Med Genet A.* 2008;146A:2145–51.
  56. Hayashi S, Okamoto N, Chinen Y, Takanashi J, Makita Y, Hata A, et al. Novel intragenic duplications and mutations of CASK in patients with mental retardation and microcephaly with pontine and cerebellar hypoplasia (MICPCH). *Hum Genet.* 2012;131(11):99–110.
  57. Hayashi S, Uehara DT, Tanimoto K, Mizuno S, Chinen Y, Fukumura S, et al. Comprehensive investigation of CASK mutations and other genetic etiologies in 41 patients with intellectual disability and microcephaly with pontine and cerebellar hypoplasia (MICPCH). *PLoS One.* 2017;12.
  58. Henikoff & Henikoff. Amino acid substitution matrices from protein blocks. *Proc Natl Acad Sci USA.* 1992;89:10915–9.
  59. Hsueh YP. The role of the MAGUK protein CASK in neural development and synaptic function. *Curr Med Chem.* 2006;13:1915–27.
  60. Hsueh YP, Wang TF, Yang FC, Sheng M. Nuclear translocation and transcription regulation by the membrane-associated guanylate kinase CASK/LIN-2. *Nature.* 2000;404(6775):298–302.
  61. Hu Y, Flockhart I, Vinayagam A, Bergwitz C, Berger B, Perrimon N, Mohr SE. An integrative approach to ortholog prediction for disease-focused and other functional studies. *BMC Bioinformatics.* 2011;31(12):357.

62. Huang TN, Chang HP, Hsueh YP. CASK phosphorylation by PKA regulates the protein-protein interactions of CASK and expression of the NMDAR2b gene. *J Neurochem*. 2010;112:1562–73.
63. Huang W, Zhou Z, Asrar S, Henkelman M, Xie W, Jia Z. p21-Activated kinases 1 and 3 control brain size through coordinating neuronal complexity and synaptic properties. *Mol Cell Biol*. 2011;31:388–403.
64. Iossifov I, O’Roak BJ, Sanders SJ, Ronemus M, Krumm N, Levy D, et al. The contribution of de novo coding mutations to autism spectrum disorder. *Nature*. 2014;515(7526):216–21.
65. Ito K, Awano W, Suzuki K, Hiromi Y, Yamamoto D. The *Drosophila* mushroom body is a quadruple structure of clonal units each of which contains a virtually identical set of neurones and glial cells. *Development*. 1997;124(4):761–71.
66. Ito K, Shinomiya K, Ito M, Armstrong JD, Boyan G, Hartenstein V, et al. A systematic nomenclature for the insect brain. *Neuron*. 2014;81(4):755–65.
67. Iyengar BG, Chou CJ, Sharma A, Atwood HL. Modular neuropile organization in the *Drosophila* larval brain facilitates identification and mapping of central neurons. *J Comp Neurol*. 2006;499:583–602.
68. Jiang L, Kraft R, Restifo L, Zohar Y. Dissociation of brain tissue into viable single neurons in a microfluidic device. *IEEE Nano/Molecular Medicine & Engineering*. 2015;9:29–32.
69. Kang HJ, Kawasawa YI, Cheng F, Zhu Y, Xu X, Li M, et al. Spatio-temporal transcriptome of the human brain. *Nature*. 2011;478:483–9.
70. Kaufmann WE, Moser HW. Dendritic anomalies in disorders associated with mental retardation. *Cereb Cortex*. 2000;10:981–91.
71. Kerr A, Patel PA, LaConte LEW, Liang C, Chen CK, Shah V, et al. Non-cell autonomous roles for CASK in optic nerve hypoplasia. *Invest Ophthalmol Vis Sci*. 2019;60:3584–94.
72. Kim MD, Wen Y, Jan YN. Patterning and organization of motor neuron dendrites in the *Drosophila* larva. *Dev Biol*. 2009;336:213–21.
73. Kingsmore SF, Smith LD, Kunard CM, Bainbridge M, Batalov S, Benson W, et al. A genome sequencing system for universal newborn screening, diagnosis, and precision medicine for severe genetic diseases. *Am J Hum Genet*. 2022;109:1605–19.
74. Kraft R, Escobar MM, Narro ML, Kurtis JL, Efrat A, Barnard K, et al. Phenotypes of *Drosophila* brain neurons in primary culture reveal a role for fascin in neurite shape and trajectory. *J Neurosci*. 2006;26:8734–47.
75. Kraft R, Kahn A, Medina-Franco JL, Orłowski ML, Baynes C, López-Vallejo F, et al. A cell-based fascin bioassay identifies compounds with potential anti-metastasis or cognition-enhancing functions. *Dis Model Mech*. 2013;6:217–35.
76. Kraft R, Levine RB, Restifo LL. The steroid hormone 20-hydroxyecdysone enhances neurite growth of *Drosophila* mushroom body neurons isolated during metamorphosis. *J Neurosci*. 1998;18:8886–99.
77. Krog CH, Agerholm JS, Nielsen SS. Fetal age assessment for Holstein cattle. *PLoS ONE*. 2018;13(11): e0207682.
78. Kulkarni VA, Firestein BL. The dendritic tree and brain disorders. *Mol Cell Neurosci*. 2012;50(1):10–20.
79. LaConte LE, Chavan V, Liang C, Willis J, Schönhense EM, Schoch S, et al. CASK stabilizes neurexin and links it to liprin- $\alpha$  in a neuronal activity-dependent manner. *Cell Mol Life Sci*. 2016;73:3599–621.
80. LaConte LEW, Chavan V, DeLuca S, Rubin K, Malc J, Berry S, et al. An N-terminal heterozygous missense CASK mutation is associated with microcephaly and bilateral retinal dystrophy plus optic nerve atrophy. *Am J Med Genet A*. 2019;179:94–103.
81. LaConte LEW, Chavan V, Elias AF, Hudson C, Schwanke C, Styren K, et al. Two microcephaly-associated novel missense mutations in CASK specifically disrupt the CASK-neurexin interaction. *Hum Genet*. 2018;137:231–46.
82. LaConte L, Mukherjee K. Structural constraints and functional divergences in CASK evolution. *Biochem Soc Trans*. 2013;41:1017–22.
83. Lai D, Gade M, Yang E, Koh HY, Lu J, Walley NM, et al. Somatic variants in diverse genes leads to a spectrum of focal cortical malformations. *Brain*. 2022;145(8):2704–20.
84. Latallo MJ, Livingston NM, Wu B. Translation imaging of single mRNAs in established cell lines and primary cultured neurons. *Methods*. 2019;162–163:12–22.
85. Laverty HG, Wilson JB. Murine CASK is disrupted in a sex-linked cleft palate mouse mutant. *Genomics*. 1998;53:29–41.
86. Lefevre G. The polytene chromosomes. In: Ashburner M, Novitski E, editors. *Genetics and Biology of Drosophila*, vol. 1a. London: Academic Press; 1976. p. 31–66.
87. Lewis S. Functions of *Drosophila Pak* (p21-activated kinase) in morphogenesis: A mechanistic model based on cellular, molecular, and genetic studies. Tucson: Doctoral dissertation, University of Arizona; 2015.
88. Liang C, Kerr A, Qiu Y, Cristofoli F, Van Esch H, Fox MA, et al. Optic nerve hypoplasia is a pervasive subcortical pathology of visual system in neonates. *Invest Ophthalmol Vis Sci*. 2017;58:5485–96.
89. Lin DM, Goodman CS. Ectopic and increased expression of Fasciclin II alters motoneuron growth cone guidance. *Neuron*. 1994;13(3):507–23. [https://doi.org/10.1016/0896-6273\(94\)90022-1](https://doi.org/10.1016/0896-6273(94)90022-1).
90. Link N, Bellen HJ. Using *Drosophila* to drive the diagnosis and understand the mechanisms of rare human diseases. *Development*. 2020;147(21):dev191411. <https://doi.org/10.1242/dev.191411>.
91. Lindsley D, Zimm G. *The Genome of Drosophila melanogaster*. San Diego: Academic Press; 1992.
92. Lopes C, Gassanova S, Delabar JM, Rachidi M. The CASK/Lin-2 *Drosophila* homologue, Camguk, could play a role in epithelial patterning and in neuronal targeting. *Biochem Biophys Res Commun*. 2001;284:1004–10.
93. Lombardo JA, Aliaghaei M, Nguyen QH, Kessenbrock K, Haun JB. Microfluidic platform accelerates tissue processing into single cells for molecular analysis and primary culture models. *Nat Commun*. 2021;12:2858.
94. Madeira F, Pearce M, Tivey ARN, Basutkar P, Lee J, Edbali O, et al. Search and sequence analysis tools services from EMBL-EBI in 2022. *Nucleic Acids Res*. 2022;50(W1):W276–9.
95. Malik BR, Gillespie JM, Hodge JJ. CASK and CaMKII function in the mushroom body  $\alpha'/\beta'$  neurons during *Drosophila* memory formation. *Front Neural Circuits*. 2013;7:52.
96. Martin JR, Ollo R. A new *Drosophila* Ca<sup>2+</sup>/calmodulin-dependent protein kinase (Caki) is localized in the central nervous system and implicated in walking speed. *EMBO J*. 1996;15:1865–76.
97. McBride SM, Holloway SL, Jongens TA. Using *Drosophila* as a tool to identify pharmacological therapies for fragile X syndrome. *Drug Discov Today Technol*. 2013;10:e129–36.
98. McKhann GM, Ho W, Raiborn C, Varon S. The isolation of neurons from normal and abnormal human cerebral cortex. *Arch Neurol*. 1969;20:542–7.
99. McSweeney D, Gabriel R, Jin K, Pang ZP, Aronow B, Pak C. CASK loss of function differentially regulates neuronal maturation and synaptic function in human induced cortical excitatory neurons. *iScience*. 2022;25(10):105187. <https://doi.org/10.1016/j.isci.2022.105187>.
100. Michaud JL, Lachance M, Hamdan FF, Carmant L, Lortie A, Diadori P, et al. The genetic landscape of infantile spasms. *Hum Mol Genet*. 2014;23(18):4846–58.
101. Molnár E. Long-term potentiation in cultured hippocampal neurons. *Semin Cell Dev Biol*. 2011;22:506–13.
102. Moog U, Kutsche K. CASK Disorders. 2013 [Updated 2020 May 21]. In: Adam MP, Everman DB, Mirzaa GM, et al., editors. *GeneReviews*<sup>®</sup> [Internet]. Seattle (WA): University of Washington, Seattle; 1993–2023. <https://www.ncbi.nlm.nih.gov/books/NBK169825/>. Accessed 10 Jan 2023.
103. Moog U, Bierhals T, Brand K, Bautsch J, Biskup S, Brune T, et al. Phenotypic and molecular insights into CASK-related disorders in males. *Orphanet J Rare Dis*. 2015;10:44.
104. Moog U, Kutsche K, Kortüm F, Chilian B, Bierhals T, Apeshioti N, et al. Phenotypic spectrum associated with CASK loss-of-function mutations. *J Med Genet*. 2011;48:741–51.
105. Mori T, Kasem EA, Suzuki-Kouyama E, Cao X, Li X, Kurihara T, et al. Deficiency of calcium/calmodulin-dependent serine protein kinase disrupts the excitatory-inhibitory balance of synapses by down-regulating GluN2B. *Mol Psychiatry*. 2019;24(7):1079–92.
106. Mukherjee K. CASK. In: Choi, S. (eds) *Encyclopedia of Signaling Molecules*. Springer, Cham. 2018; [https://doi.org/10.1007/978-3-319-67199-4\\_101833](https://doi.org/10.1007/978-3-319-67199-4_101833).
107. Mukherjee K, LaConte LEW, Srivastava S. The non-linear path from gene dysfunction to genetic disease: lessons from the MICPCH mouse model. *Cells*. 2022;11(7).

108. Mukherjee K, Patel PA, Rajan DS, LaConte LEW, Srivastava S. Survival of a male patient harboring CASK Arg27Ter mutation to adolescence. *Mol Genet Genomic Med.* 2020;8(10): e1426.
109. Mukherjee K, Sharma M, Urlaub H, Bourenkov GP, Jahn R, Südhof TC, et al. CASK Functions as a Mg<sup>2+</sup>-independent neurexin kinase. *Cell.* 2008;133:328–39.
110. Mukherjee K, Slawson JB, Christmann BL, Griffith LC. Neuron-specific protein interactions of *Drosophila* CASK-beta are revealed by mass spectrometry. *Front Mol Neurosci.* 2014;7:58.
111. Muthusamy B, Selvan LDN, Nguyen TT, Manoj J, Stawiski EW, Jaiswal BS, et al. Next-generation sequencing reveals novel mutations in X-linked intellectual disability. *OMICS.* 2017;21:295–303.
112. Najm J, Horn D, Wimplinger I, Golden JA, Chizhikov VV, Sudi J, et al. Mutations of CASK cause an X-linked brain malformation phenotype with microcephaly and hypoplasia of the brainstem and cerebellum. *Nat Genet.* 2008;40:1065–7.
113. Nakajiri T, Kobayashi K, Okamoto N, Oka M, Miya F, Kosaki K, et al. Late-onset epileptic spasms in a female patient with a CASK mutation. *Brain Dev.* 2015;37(9):919–23.
114. Napolitano T, Holford M. Breakthroughs in venom peptide screening methods to advance future drug discovery. *Protein Pept Lett.* 2018;25(12):1137–48.
115. Narro ML, Yang F, Kraft R, Wenk C, Efrat A, Restifo LL. NeuronMetrics: software for semi-automated processing of cultured neuron images. *Brain Res.* 2007;1138:57–75.
116. Neuhaus W, Reininger-Gutmann B, Rinner B, Plasenzotti R, Wilflingseder D, De Kock J, et al. The rise of Three Rs centres and platforms in Europe. *Altern Lab Anim.* 2022;50:90–120.
117. Nicholls DG, Brand MD, Gerencser AA. Mitochondrial bioenergetics and neuronal survival modelled in primary neuronal culture and isolated nerve terminals. *J Bioenerg Biomembr.* 2015;47:63–74.
118. Nuovo S, Micalizzi A, Romaniello R, Arrigoni F, Ginevrino M, Casella A, et al. Refining the mutational spectrum and gene-phenotype correlates in pontocerebellar hypoplasia: results of a multicentric study. *J Med Genet.* 2022;59(4):399–409.
119. Pan YE, Tibbe D, Harms FL, Reißner C, Becker K, Dingmann B, et al. Missense mutations in CASK, coding for the calcium-/calmodulin-dependent serine protein kinase, interfere with neurexin binding and neurexin-induced oligomerization. *J Neurochem.* 2021;157:1331–50.
120. Patel PA, Hegert JV, Cristian I, Kerr A, LaConte LEW, Fox MA, et al. Complete loss of the X-linked gene. *J Med Genet.* 2022;59:1044–57.
121. Patel PA, Liang C, Arora A, Vijayan S, Ahuja S, Wagley PK, et al. Haploinsufficiency of X-linked intellectual disability gene CASK induces post-transcriptional changes in synaptic and cellular metabolic pathways. *Exp Neurol.* 2020;329: 113319.
122. Peruffo A, Cozzi B. Bovine brain: An in vitro translational model in developmental neuroscience and neurodegenerative research. *Front Pediatr.* 2014;2:74.
123. Pexsters A, Daemen A, Bottomley C, Van Schoubroeck D, De Catte L, De Moor B, et al. New crown-rump length curve based on over 3500 pregnancies. *Ultrasound Obstet Gynecol.* 2010;35:650–5.
124. Piluso G, D'Amico F, Saccone V, Bismuto E, Rotundo IL, Di Domenico M, et al. A missense mutation in CASK causes FG syndrome in an Italian family. *Am J Hum Genet.* 2009;84:162–77.
125. Prem S, Millonig JH, DiCicco-Bloom E. Dysregulation of neurite outgrowth and cell migration in autism and other neurodevelopmental disorders. *Adv Neurobiol.* 2020;25:109–53.
126. Qu J, Zhou Y, Li Y, Yu J, Wang W. CASK regulates Notch pathway and functions as a tumor promoter in pancreatic cancer. *Arch Biochem Biophys.* 2021;701: 108789.
127. R Core Team. R: A language and environment for statistical computing. R Foundation for Statistical Computing, Vienna, Austria. 2022. <https://www.R-project.org/>. Accessed 15 Dec 2022.
128. Rama Devi AR, Lingappa L, Naushad SM. Identification and *in silico* characterization of a novel CASK c.2546T>C (p.V849A) mutation in a male infant with pontocerebellar hypoplasia. *Ann Indian Acad Neurol.* 2019;22:523–4.
129. Rivas L, Blanco Ó, Torreira C, Repáraz A, Melcón C, Amado A [Pontocerebellar hypoplasia secondary to CASK gene deletion: Case report]. *Rev Chil Pediatr.* 2017;88:529–33.
130. Riveros AJ, Gronenberg W. Brain allometry and neural plasticity in the bumblebee *Bombus occidentalis*. *Brain Behav Evol.* 2010;75:138–48.
131. Robinow S, White K. The locus *elav* of *Drosophila melanogaster* is expressed in neurons at all developmental stages. *Dev Biol.* 1988;126:294–303.
132. Robinow S, White K. Characterization and spatial distribution of the ELAV protein during *Drosophila melanogaster* development. *J Neurobiol.* 1991;22(5):443–61.
133. Russ N, Schröder M, Berger BT, Mandel S, Aydogan Y, Mauer S, et al. Design and development of a chemical probe for pseudokinase Ca<sup>2+</sup>/calmodulin-dependent Ser/Thr kinase. *J Med Chem.* 2021;64:14358–76.
134. Saleem R, Setty G, Hussain N. MICrocephaly, disproportionate pontine and cerebellar hypoplasia syndrome: a clinico-radiologic phenotype linked to calcium/calmodulin-dependent serine protein kinase gene mutation. *Indian J Hum Genet.* 2013;19:104–7.
135. Samuels BA, Hsueh YP, Shu T, Liang H, Tseng HC, Hong CJ, et al. Cdk5 promotes synaptogenesis by regulating the subcellular distribution of the MAGUK family member CASK. *Neuron.* 2007;56:823–37.
136. Saumweber T, Rohwedder A, Schleyer M, Eichler K, Chen YC, Aso Y, et al. Functional architecture of reward learning in mushroom body extrinsic neurons of larval *Drosophila*. *Nat Commun.* 2018;9:1104.
137. Schneider CA, Rasband WS, Eliceiri KW. NIH Image to ImageJ: 25 years of image analysis. *Nat Methods.* 2012;9:671–5.
138. Scorza WE, Vintzileos A. First and second trimester sonography: an American perspective. *Int J Fertil Menopausal Stud.* 1996;41(3):288–92.
139. Seto T, Hamazaki T, Nishigaki S, Kudo S, Shintaku H, Ondo Y, et al. A novel CASK mutation identified in siblings exhibiting developmental disorders with/without microcephaly. *Intractable Rare Dis Res.* 2017;6:177–82.
140. Shembekar N, Hu H, Eustace D, Merten CA. Single-cell droplet microfluidic screening for antibodies specifically binding to target cells. *Cell Rep.* 2018;22:2206–15.
141. Sia SK, Whitesides GM. Microfluidic devices fabricated in poly(dimethylsiloxane) for biological studies. *Electrophoresis.* 2003;24:3563–76.
142. Slawson JB, Kuklin EA, Ejima A, Mukherjee K, Ostrovsky L, Griffith LC. Central regulation of locomotor behavior of *Drosophila melanogaster* depends on a CASK isoform containing CaMK-like and L27 domains. *Genetics.* 2011;187:171–84.
143. Smrt RD, Lewis SA, Kraft R, Restifo LL. Primary culture of *Drosophila* larval neurons with morphological analysis using NeuronMetrics. *Drosophila Inf Serv.* 2015;98:125–40. <https://www.ou.edu/journals/dis/DIS98/TeachInf/Smrt%20et%20al.pdf>. Accessed 20 Aug 2023.
144. Spokony RF, Restifo LL. Broad Complex isoforms have unique distributions during central nervous system metamorphosis in *Drosophila melanogaster*. *J Comp Neurol.* 2009;517:15–36.
145. Srivastava S, McMillan R, Willis J, Clark H, Chavan V, Liang C, et al. X-linked intellectual disability gene CASK regulates postnatal brain growth in a non-cell autonomous manner. *Acta Neuropathol Commun.* 2016;4:30.
146. Sun B, Salvaterra PM. Characterization of nervana, a *Drosophila melanogaster* neuron-specific glycoprotein antigen recognized by anti-horseradish peroxidase antibodies. *J Neurochem.* 1995;65:434–43.
147. Sun M, Liu L, Zeng X, Xu M, Fang M, Xie W. Genetic interaction between Neurexin and CASK/CMG is important for synaptic function in *Drosophila* neuromuscular junction. *Neurosci Res.* 2009;64:362–71.
148. Takanashi J, Arai H, Nabatame S, Hirai S, Hayashi S, Inazawa J, et al. Neuro-radiologic features of CASK mutations. *AJNR Am J Neuroradiol.* 2010;31:1619–22.
149. Takanashi J, Okamoto N, Yamamoto Y, Hayashi S, Arai H, Takahashi Y, et al. Clinical and radiological features of Japanese patients with a severe phenotype due to CASK mutations. *Am J Med Genet A.* 2012;158A:3112–8.
150. Tarpey PS, Smith R, Pleasance E, Whibley A, Edkins S, Hardy C, et al. A systematic, large-scale resequencing screen of X-chromosome coding exons in mental retardation. *Nat Genet.* 2009;41:535–43.
151. Tibbe D, Ferle P, Krisp C, Nampoothiri S, Mirzaa G, Assaf M, et al. Regulation of Liprin- $\alpha$  phase separation by CASK is disrupted by a mutation in its CaM kinase domain. *Life Sci Alliance.* 2022;5.

152. Titmarsh DM, Glass NR, Mills RJ, Hidalgo A, Wolvetang EJ, Porrello ER, et al. Induction of human iPSC-derived cardiomyocyte proliferation revealed by combinatorial screening in high density microbio-reactor arrays. *Sci Rep*. 2016;6:24637.
153. Valayannopoulos V, Michot C, Rodriguez D, Hubert L, Saillour Y, Labrune P, et al. Mutations of TSEN and CASK genes are prevalent in pontocerebellar hypoplasias type 2 and 4. *Brain*. 2012;135(Pt 1):e199; author reply e200.
154. Verstraelen P, Van Dyck M, Verschuuren M, Kashikar ND, Nuydens R, Timmermans JP, et al. Image-based profiling of synaptic connectivity in primary neuronal cell culture. *Front Neurosci*. 2018;12:389.
155. Varon S, Raiborn CW. Dissociation, fractionation, and culture of embryonic brain cells. *Brain Res*. 1969;12:180–99.
156. Vincent AM, Feldman EL. Can drug screening lead to candidate therapies for testing in diabetic neuropathy? *Antioxid Redox Signal*. 2008;10:387–93.
157. Watkins RJ, Patil R, Goult BT, Thomas MG, Gottlob I, Shackleton S. A novel interaction between FRMD7 and CASK: evidence for a causal role in idiopathic infantile nystagmus. *Hum Mol Genet*. 2013;22:2105–18.
158. Wei JL, Fu ZX, Fang M, Zhou QY, Zhao QN, Guo JB, et al. High expression of CASK correlates with progression and poor prognosis of colorectal cancer. *Tumour Biol*. 2014;35:9185–94.
159. Whitton DS. Drug discovery for hearing loss: Phenotypic screening of chemical compounds on primary cultures of the spiral ganglion. *Hear Res*. 2017;349:177–81.
160. Wincent J, Kolbjørn S, Martin D, Luthman A, Åmark P, Dahlin M, et al. Copy number variations in children with brain malformations and refractory epilepsy. *Am J Med Genet A*. 2015;167A:512–23.
161. Wright CF, FitzPatrick DR, Firth HV. Paediatric genomics: diagnosing rare disease in children. *Nat Rev Genet*. 2018;19(5):325.
162. Wu Z, Hjort K, Wicher G, Svenningsen AF. Microfluidic high viability neural cell separation using viscoelastically tuned hydrodynamic spreading. *Biomed Microdevices*. 2008;10:631–8.
163. Yaginuma K, Aoki W, Miura N, Ohtani Y, Aburaya S, Kogawa M, et al. High-throughput identification of peptide agonists against GPCRs by co-culture of mammalian reporter cells and peptide-secreting yeast cells using droplet microfluidics. *Sci Rep*. 2019;9:10920.
164. Yamazaki W, Takahashi M, Kawahara M. Restricted development of mouse triploid fetuses with disorganized expression of imprinted genes. *Zygote*. 2015;23:874–84.
165. Yavin E, Menkes JH. The culture of dissociated cells from rat cerebral cortex. *J Cell Biol*. 1973;57:232–7.
166. Zheng XT, Yu L, Li P, Dong H, Wang Y, Liu Y, et al. On-chip investigation of cell-drug interactions. *Adv Drug Deliv Rev*. 2013;65:1556–74.
167. Zhou X, Xu G, Yin C, Jin W, Zhang G. Down-regulation of miR-203 induced by *Helicobacter pylori* infection promotes the proliferation and invasion of gastric cancer by targeting CASK. *Oncotarget*. 2014;5:11631–40.
168. Zordan MA, Massironi M, Ducato MG, Te Kronnie G, Costa R, Reggiani C, et al. Drosophila CAKI/CMG protein, a homolog of human CASK, is essential for regulation of neurotransmitter vesicle release. *J Neurophysiol*. 2005;94:1074–83.

## Publisher's Note

Springer Nature remains neutral with regard to jurisdictional claims in published maps and institutional affiliations.

Ready to submit your research? Choose BMC and benefit from:

- fast, convenient online submission
- thorough peer review by experienced researchers in your field
- rapid publication on acceptance
- support for research data, including large and complex data types
- gold Open Access which fosters wider collaboration and increased citations
- maximum visibility for your research: over 100M website views per year

At BMC, research is always in progress.

Learn more [biomedcentral.com/submissions](https://biomedcentral.com/submissions)

